Available online at www.sciencedirect.com

ScienceDirect

Geochimica et Cosmochimica Acta 125 (2014) 1–22

Geochimica et Cosmochimica Acta

www.elsevier.com/locate/gca

Partitioning of copper between olivine, orthopyroxene, clinopyroxene, spinel, garnet and silicate melts at upper mantle conditions

Xingcheng Liu [a,c], Xiaolin Xiong [a,d,*], Andreas Audétat [b], Yuan Li [b], Maoshuang Song [a], Li Li [a,c], Weidong Sun [d], Xing Ding [a]

[a] State Key Laboratory of Isotope Geochemistry, Guangzhou Institute of Geochemistry, Chinese Academy of Sciences, Guangzhou 510640, China

[b] Bayerisches Geoinstitut, Universität Bayreuth, D-95440 Bayreuth, Germany

[c] University of the Chinese Academy of Sciences, Beijing 100049, China

[d] Key Laboratory of Mineralogy and Metallogeny, Guangzhou Institute of Geochemistry, Chinese Academy of Sciences, Guangzhou 510640, China

Received 5 May 2013; accepted in revised form 27 September 2013; Available online 10 October 2013

Abstract

Previously published Cu partition coefficients (D_{Cu}) between silicate minerals and melts cover a wide range and have resulted in large uncertainties in model calculations of Cu behavior during mantle melting. In order to obtain true $D_{Cu}^{mineral/melt}$ values, this study used $Pt_{95}Cu_{05}$ alloy capsules as the source of Cu to experimentally determine the D_{Cu} between olivine (ol), orthopyroxene (opx), clinopyroxene (cpx), spinel (spl), garnet (grt) and hydrous silicate melts at upper mantle conditions. Three synthetic silicate compositions, a Komatiite, a MORB and a $Di_{70}An_{30}$, were used to produce these minerals and melts. The experiments were conducted in piston cylinder presses at 1.0–3.5 GPa, 1150–1300 °C and oxygen fugacities (fO_2) of from ~2 log units below to ~5 log units above fayalite–magnetite–quartz (FMQ). The compositions of minerals and quenched melts in the run products were measured with EMP and LA-ICP-MS. Attainment of equilibrium is verified by reproducible D_{Cu} values obtained at similar experimental conditions but different durations. The results show that D_{Cu} for ol/, opx/, spl/ and possibly cpx/melt increase with increasing fO_2 when $fO_2 > FMQ + 1.2$, while D_{Cu} for cpx/ and spl/melt also increase with increasing Na_2O in cpx and Fe_2O_3 in spinel, respectively. In the investigated P–T–fO_2 conditions, the $D_{Cu}^{mineral/melt}$ values are 0.04–0.14 for ol, 0.04–0.09 for opx, 0.02–0.23 for cpx, 0.19–0.77 for spl and 0.03–0.05 for grt. These results confirm that Cu is highly incompatible ($D_{Cu} < \sim 0.2$) in all the silicate minerals and oxides of the upper mantle with the exception of the high-Fe spinel, in which Cu is moderately incompatible ($D_{Cu} = 0.4–0.8$) and thus Cu will be enriched in the derived melts during mantle partial melting and magmatic differentiation if sulfide is absent. These experimental D_{Cu} values are used to assess the controls on Cu behavior during mantle melting. The model results suggest that MORBs and most arc basalts must form by sulfide-present melting at relatively reduced conditions, while high Cu (>70 ppm) arc basalts may form at oxidized, sulfide-absent conditions, which is consistent with the possibility of some high fO_2 regions present in the arc mantle.

1. INTRODUCTION

The partition coefficients of Cu between minerals and melts ($D_{Cu}^{mineral/melt}$) have broad applications for studies of crust–mantle differentiation and formations of magmatic

* Corresponding author at: State Key Laboratory of Isotope Geochemistry, Guangzhou Institute of Geochemistry, Chinese Academy of Sciences, Guangzhou 510640, China. Tel.: +86 20 8529 0287.

E-mail address: xiongxl@gig.ac.cn (X. Xiong).

0016-7037/$ - see front matter © 2013 Elsevier Ltd. All rights reserved.
http://dx.doi.org/10.1016/j.gca.2013.09.039

and magmatic-hydrothermal ore deposits (Audetat and Pettke, 2006; Sinclair, 2007; Jenner et al., 2010; Fellows and Canil, 2012; Lee et al., 2012). The primitive upper mantle has an estimated Cu abundance of 20–30 ppm (Sun, 1982; O'Neill, 1991). Mantle-derived primitive basaltic magmas (MgO > 8 wt.%) such as mid-ocean ridge basalts (MORB), arc basalts (AB) and ocean island basalts (OIB) have Cu concentrations generally in the range of 60–80, 50–100 and 80–120 ppm, respectively (Fellows and Canil, 2012; Lee et al., 2012). This suggests that Cu behaves incompatibly during partial melting of the mantle. The upper mantle consists mostly of olivine, opx, cpx and an Al-rich phase (garnet or spinel or plagioclase), with possibly minor sulfides. As a chalcophile element, the behavior of Cu during mantle melting or magma evolution could potentially be dominated by sulfide phases, because the Cu partition coefficient between sulfide phases and silicate melts ranges from several hundreds to over a thousand (Naldrett, 1989; Gaetani and Grove, 1997; Ripley et al., 2002; Li and Audétat, 2012). Cu behavior during mantle melting is controlled by bulk $D_{Cu}^{residue/melt}$ (residue = silicate minerals + sulfides). Although minor sulfide has a substantial contribution to the bulk D_{Cu}, silicate minerals could potentially have a strong effect on the bulk D_{Cu}, provided that corresponding mineral–melt partition coefficients are high enough. Silicate minerals will also dominate the behavior of Cu when sulfides are absent, such as at high degrees of partial melting after sulfides became completely exhausted or at a high fO_2 (>FMQ + 2) that destabilize sulfides (Carroll and Rutherford, 1987; Jugo et al., 2005, 2010). In addition, at the early stages of crystallization of mantle-derived magmas emplaced in the crust and surface, the behavior of Cu is also entirely controlled by silicate minerals since sulfide-saturated magmas ascending from depth tend to become sulfide-unsaturated due to the increase of sulfur solubility in the melt with decreasing pressure (Mavrogenes and O'Neill, 1999). Therefore, accurate Cu partition coefficients between silicate minerals and melts are required for a quantitative understanding of the behavior of Cu during mantle melting and magmatic differentiation.

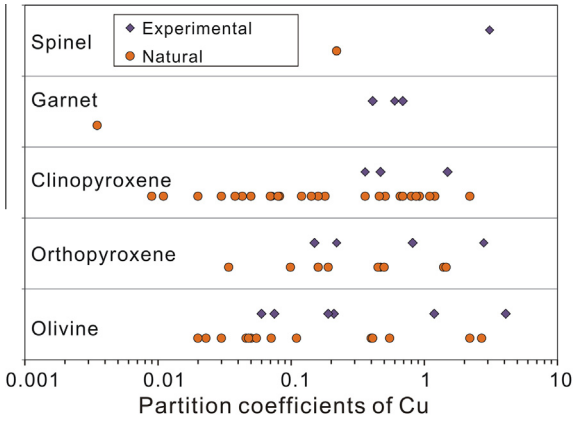

Fig. 1. Literature D_{Cu} values between mantle minerals and silicate melts determined with natural phenocryst–matrix samples and experimental run products (see Table S1 for the data list). Natural phenocryst–matrix D_{Cu} values from Audetat and Pettke (2006), Bougault and Hekinian (1974), De Hoog et al. (2001), Dostal et al. (1983), Ewart et al. (1973), Ewart and Griffin (1994), Halter et al.(2004), Kloeck and Palme (1987), Lee et al. (2012), Paster et al. (1974), Pedersen (1979), Zack and Brumm (1998), Zajacz and Halter (2007). Experimental D_{Cu} values from Adam and Green (2006), Fellows and Canil (2012), Gaetani and Grove (1997), Hart and Dunn (1993), Klemme et al. (2006), Yurimoto and Ohtani (1992).

However, published Cu partitioning data between mantle silicate minerals and melts (Fig. 1, See Table S1 for the details) are internally inconsistent, discrete and even paradoxical. As shown in Fig. 1, published mantle minerals/melts D_{Cu} values vary by over two orders of magnitude, ranging from 0.02 to 4.1 for olivine/, 0.03 to 2.8 for opx/, 0.03 to 1.5 for cpx/, 0.004 to 0.69 for garnet/ and 0.22 to 3.1 for spinel/melt pairs. Obviously, the >1.0 D_{Cu} values for key minerals olivine, opx and cpx appear to be in conflict with the incompatible behavior of Cu during mantle melting. The published D_{Cu} values were obtained with natural phenocryst–matrix samples or experimental mineral–melt (quenched glass) products (Table S1). Most of the early phenocryst–matrix D_{Cu} values were obtained by analyzing glasses and mineral separates, which would probably contain tiny sulfide inclusions leading to much higher D_{Cu} than the true values. In contrast, the D_{Cu} values for most mantle silicate minerals obtained recently with the in situ LA-ICP-MS analysis of natural phenocryst and matrix pairs (Audetat and Pettke, 2006; Lee et al., 2012) are much lower (<0.1, see Table S1), which are distinctly different from the old data. Experimental study provides another approach for obtaining Cu partition coefficients at controlled conditions (Hart and Dunn, 1993; Gaetani and Grove, 1997; Klemme et al., 2006; Adam and Green, 2006; Fellows and Canil, 2012). However, most experimentally determined silicate mineral/melt D_{Cu} values published so far are associated with considerable uncertainty because they were obtained from experiments conducted with Cu-free noble metal capsules. Similar to Fe, Cu easily alloys with noble metal capsules during high P–T experiments (Zajacz et al., 2012), especially at reduced conditions such as those imposed by the graphite buffer (Fellows and Canil, 2012). Continuous Cu loss from sample charges into noble metal capsule walls during experiments not only leads to very low concentrations of Cu in the run products and therefore increases analytical uncertainty, but also disturbs the Cu partitioning equilibrium between minerals and melts. This is because Cu diffusion in a melt is expected to be much faster than in a coexisting mineral crystal, which will unavoidably result in faster loss of Cu from the melt than from the mineral into the capsule wall. If Cu loss keeps going after crystallization has stopped, then this will lead to a higher D_{Cu} than the true value.

The wide range of D_{Cu} values previously published for silicate minerals have resulted in large uncertainties in model calculations. Two opposite and mutually exclusive papers (Lee et al., 2012; Fellows and Canil, 2012) came out last year. Lee et al. (2012) using natural mineral/melt partition coefficients ($D_{Cu}^{ol/melt} = 0.05$, ($D_{Cu}^{opx/melt} = 0.035$, ($D_{Cu}^{cpx/melt} = 0.04$) concluded that Cu is highly incompatible in silicate phases and thus residual sulfide is present during

the genesis of MORBs and arc basalts. However, experimental results from Fellows and Canil (2012) show that Cu is moderately incompatible in olivine ($D_{Cu} = 0.06$–0.21) and opx ($D_{Cu} = 0.15$–0.82) and their model calculations suggest that MORB and arc basalts can be produced at sulfide-absent conditions. Hence, applications of different D_{Cu} values have resulted in fundamentally different interpretation of the control on Cu behavior.

In order to obtain better and more accurate Cu partitioning data for silicate minerals, we here use $Pt_{95}Cu_{05}$ (95 wt.% Pt + 5 wt.% Cu) alloy capsules as the Cu source to determine the partition coefficients of Cu between olivine, opx, cpx, spinel, garnet and hydrous silicate melts. This capsule technique avoids Cu alloy problem that is common in experiments conducted with Cu-free noble metal capsules. A very similar approach was developed and successfully used to determine the solubility and partitioning behavior of Au and Cu in mafic to felsic magmas by Zajacz et al. (2011, 2012) and Zajacz et al. (2013), who employed Au97Cu3 alloy capsules to eliminate the exact same problem. Experiments in this study were conducted in piston cylinder presses at 1.0–3.5 GPa and 1150–1300 °C, with oxygen fugacity (fO_2) varying from ~2 log units below to ~5 log units above FMQ. The results were compared to previously published silicate minerals/melts D_{Cu} values and were used to model and discuss the controls of Cu behavior during the genesis of MORBs and arc basalts.

2. EXPERIMENTAL AND ANALYTICAL METHODS

2.1. Starting materials

Three compositions, a Komatiite, a MORB and a $Di_{70}An_{30}$ (Di – diopside, An – anorthite), were selected and synthetized for this study (Table 1). Komatiite and MORB were selected because they are mantle-derived melts and are easily saturated with mafic minerals at upper mantle P–T conditions. The iron-free $Di_{70}An_{30}$ composition was used to study cpx-melt partitioning. These compositions were prepared by mixing together reagent grade oxides SiO_2, Al_2O_3, Fe_2O_3, MgO, TiO_2, MnO, NiO, P_2O_5 and Cr_2O_3 and carbonates $CaCO_3$, Na_2CO_3 and K_2CO_3. The mixtures were ground under acetone, then sintered in Pt crucibles at 1000 °C for ten hours to remove CO_2, and then were fused in the same Pt crucibles at 1500 °C for 2 h. The quenched glasses were ground again to produce starting silicate powder. Two rounds of fusion and grinding were performed to improve chemical homogeneity. Before the second round of grinding, several aliquots of the quenched glasses were left for analyses with electron microprobe (EMP). In order to monitor the analytical quality of Cu concentrations in experimentally crystallized mineral phases (for the details, see Section 2.5) with the laser ablation-inductively coupled plasma-mass spectrometry (LA-ICP-MS), the powdered starting materials were also doped with <100 ppm rubidium as rubidium hydroxide aqueous solution and then were dried at 150 °C in an oven for several hours.

Table 1
Starting compositions (wt%).

	Komatiite	MORB	$Di_{70}An_{30}$
n	8	7	9
SiO_2	45.14(0.36)	50.07(0.58)	51.18(0.54)
TiO_2	0.45(0.04)	1.66(0.05)	0.03(0.02)
Al_2O_3	10.31(0.12)	15.38(0.15)	13.28(0.18)
FeO	11.84(0.27)	10.8(0.24)	0.06(0.02)
MnO	0.17(0.01)	0.02(0.01)	0.03(0.02)
MgO	20.35(0.22)	6.80(0.11)	10.00(0.11)
CaO	9.04(0.09)	11.61(0.19)	25.33(0.31)
Na_2O	0.77(0.04)	2.83(0.11)	0.04(0.03)
K_2O	0.06(0.02)	0.23(0.02)	0.04(0.01)
P_2O_5	0.08(0.01)	0.30(0.02)	0.02(0.01)
NiO	0.23(0.03)	0.03(0.01)	0.02(0.02)
Cr_2O_3	0.50(0.03)	0.01(0.01)	0.03(0.01)
Total	98.95(0.62)	99.74(0.97)	100.06(0.94)

Note: Compositions were determined by EMP, all Fe is expressed as FeO. Numbers in brackets correspond to 1σ standard deviation.

2.2. Sample capsules and fO_2 control

$Pt_{95}Cu_{05}$ alloy capsules were selected for all experiments in this study. Two types of $Pt_{95}Cu_{05}$ alloy tubes were bought from Sino-Platinum Metals Co., Ltd (the manufacturer), one with 2.7 mm ID and 3.0 mm OD, the other with 4.7 mm ID and 5.0 mm OD. As determined by the manufacturer, Cu concentration in all the alloy tubes is homogeneous with exactly 94.74 wt.% Pt and 5.26 wt.% Cu. The smaller tubes were used to make sample capsules (sample containers) and the larger ones were used to make capsules to hold the sample capsules and oxygen buffer materials. About 15 mg starting silicate powder was loaded into each of the sample capsules which have a mass range of 180–250 mg before the samples were filled. During the experiments, Cu quickly diffused from the capsule into the melted sample and the apparent solubility of Cu in the melt was controlled by the partitioning between the capsule and the melt. As the mass of a capsule is 12–16 times higher than the mass of the silicate charge enclosed, and given that Cu highly partitioned toward the capsule alloy, the composition and Cu activity of the capsule were nearly unchanged during the experiments. Thus the activity or the concentration of Cu in each phase of the charge at a given P–T–fO_2 condition should be buffered at a constant value by the capsule alloy. In addition to the 15 mg silicate powder, <5.0 wt.% H_2O was also loaded into the capsules. These capsules (except those with graphite buffer, see below) then were welded shut, and were dried to check possible leakage. The H_2O added to the sample charges helps to promote distribution equilibrium and crystal growth during the experiments.

Three capsule configurations were used to impose different levels of fO_2 on the samples. (1) For the experiments at reducing conditions, graphite buffer was used (Table 2). A sample-containing capsule was first loaded into a graphite capsule that itself was then sealed into an outer $Pt_{95}Cu_{05}$ capsule with 4.7 mm ID and 5.0 mm OD. In this setup, the inner sample capsule was welded on one end, with the other end only crimped to allow free chemical communication between the sample and the graphite. In this case, the

Table 2
Experimental conditions and run products (phase assemblages).

Run No.[a]	Starting material	H_2O Initial (%)	fO_2 Buffer	P (GPa)	T (°C)	Duration (h)	Phases [b] (wt.%)	fO_2 [c] Δ FMQ	Estimated fO_2 [d] Δ FMQ	Fe loss[e] (%)	Cu in the melt [f] (ppm)
Cu-50#	Komatiite	1.0	Graphite	1.0	1300	27	Gl (73), Ol (19), Opx (7), Spl (1)	−1.7	−1.8	70	281(8)
Cu-46#	Komatiite	1.0	–	1.0	1300	24	Gl (84), Ol (15), Spl (2)	–	3.8	6	13,271(2214)
Cu-31#	Komatiite	3.8	–	1.0	1270	49	Gl (77), Ol (4), quenched cpx(18), Spl (1)	–	3.6	11	8487(17)
Cu-5#	Komatiite	3.9	–	1.0	1250	48	Gl (67), Ol (31), Spl (3)	–	4.4	12	9343(1414)
Cu-30#	Komatiite	5.0	FMQ	1.0	1250	48	Gl (94), Ol (5), Spl (1)	0	3.9	14	5848(40)
Cu-55#	Komatiite	1.0	MnMnO	1.0	1290	26	Gl (77), Ol (3), quenched cpx(20), Spl (1)	3.6	3.5	14	13,034(559)
Komatiite-L4	Komatiite	1.3	–	1.0	1300	24	Gl (58), Ol (16), Cpx (12)Opx (14), Spl (1)	–	1.2	64	866(41)
Komatiite-L2	Komatiite	1.5	NNO	1.0	1300	23	Gl (67), Ol (33), Spl (1)	0.3	0.8	88	783(187)
Komatiite-L1	Komatiite	1.4	HM	1.0	1290	23	Gl (42), Ol (9), Opx (23), Cpx (20), Spl (6)	5.1	4.6	0	5125(655)
Cu-41#[†]	MORB	3.4	Graphite	1.0	1150	72	Gl (78), Cpx (14), Pl (8)	−1.4	<−1.4	7	1497(191)
Cu-6#	MORB	5.1	–	1.0	1150	72	Gl (76), Cpx (21), Spl (3)	–	–	0	4885(76)
MORB-L2	MORB	5.2	NNO	2.5	1250	37	Gl (80), Cpx (20)	−0.1	<−0.1	76	420(9)
MORB-L1	MORB	5.1	HM	2.5	1250	30	Gl (88), Cpx (12)	4.4	<4.4	14	4906(198)
MORB-L3	MORB	1.6	NNO	3.0	1250	58	Gl (74), Cpx (26)	−0.3	<−0.3	90	524(10)
MORB-L5	MORB	4.2	–	3.5	1200	69	Gl (46), Grt (13), Cpx (41)	–	–	9	3574(320)
MORB-L6	MORB	4.6	HM	3.5	1200	46	Gl (50), Grt (20), Cpx (30)	3.8	<3.8	9	3817(242)
Cu-35#	$Di_{70}An_{30}$	4.0	Graphite	1.0	1215	79	Gl (63), Di (37)	−1.5	<−1.5	–	107(2)
Cu-47#	$Di_{70}An_{30}$	5.0	–	1.0	1240	48	Gl (80), Di (20)	–	–	–	610(21)
Cu-52#	$Di_{70}An_{30}$	5.0	FMQ	1.0	1230	49	Gl (67), Di (33)	0	–	–	4777(228)
Cu-43#	$Di_{70}An_{30}$	5.3	FMQ	1.0	1220	48	Gl (69), Di (31)	0	–	–	5143(71)
Cu-48#	$Di_{70}An_{30}$	5.3	MnMnO	1.0	1240	38	Gl (94), Di (6)	3.6	<3.6	–	6966(123)

[a] Run numbers with # were performed at Guangzhou; the other runs were performed at Bayreuth.
[b] Abbreviations: Gl = glass, Ol = olivine, Opx = orthopyroxene, Cpx = clinopyroxene, Spl = spinel, Grt = garnet, Pl = plagioclase, and Di = diopside; the products modes were obtained by mass balance calculation.
[c] The theoretical values of fO_2 were calculated referring O'Neill and Pownceby (1993a) and Frost (1991) for NNO buffer; O'Neill and Pownceby (1993b) for MnMnO buffer; O'Neill (1987) for FMQ buffer; Haas and Robie (1973) for HM buffer; Jakobsson and Oskarsson (1994) for Graphite buffer.
[d] The estimated fO_2 were calculated using Ol-Opx-Spl oxygen geobarometer (Ballhaus et al., 1990, 1991); the uncertainties is ±0.4 log units above FMQ, and ±1.2 log units when graphite buffer was used. $Fe^{2+}/\sum Fe$ ratios were calculated, following the methods of Droop (1987), from EMPA assuming that the spinels have perfect stoichiometry; analytical data of minerals used for the calculations from Tables 4 and 6.
[e] Fe loss was calculated by mass balance using the EMP data in Tables 3–7. Fe loss (%) = 100 × (FeO in starting material − FeO calculated)/FeO in starting material.
[f] data from Table 3.
[†] Run Cu-41# is an experiment conducted with graphite-lined $Pt_{95}Cu_{05}$ capsule, within which MORB + Cu metal powder was filled and Cu partitioning equilibrium probably was not achieved completely. The results for this run are only shown for comparison.

fO_2 attained in the sample during an experiment should be consistent with the externally imposed graphite buffer. (2) For the experiments at conditions more oxidized than the graphite buffer, a conventional double-capsule technique similar to Chou (1987) and oxygen buffer materials Fayalite–Magnetite–Quartz (FMQ), Ni–NiO (NNO), MnO–Mn_3O_4 (MnMnO) or Hematite–Magnetite (HM) were employed. In this setup, a sealed sample-containing capsule was welded into an outer $Pt_{95}Cu_{05}$ capsule. The space between was filled with buffer materials and H_2O. In this setup, the fO_2 attained in the sample during the experiment should be a little lower than the externally imposed oxygen buffer because the water activity in the silicate melt was less than unity (Li and Audétat, 2012). For some of these runs fO_2 was determined after the experiment with olivine-opx-spinel oxygen geobarometer (Ballhaus et al., 1990, 1991). (3) There are seven experiments not buffered by externally imposed oxygen buffers. In this setup, a single sample capsule was inserted into the center of an MgO tube with crushable MgO spacer and powder filled into the remaining space of the tube. For these experiments, exact fO_2 values cannot be obtained except for the olivine-opx-spinel oxygen geobarometer.

2.3. High pressure and temperature experiments

All the experiments were conducted at 1.0–3.5 GPa and 1150–1300 °C with durations ranging from 23 to 78 h (Table 2). The experimental equipment was an end-loaded, solid media piston cylinder apparatus at the Guangzhou

Institute of Geochemistry or at the Bayerisches Geoinstitut. For the experiments at pressures higher than 1.5 GPa, a 1/2 inch pressure vessel was used, whereas at lower pressures, a 3/4 inch pressure vessel was used. The assembly in the pressure cell was composed of an outer talc/NaCl + Pyrex sleeve and a tapered graphite heater, inside which, the sample capsule with a pyrophyllite or MgO sleeve was positioned at the center of the heater with Al_2O_3 spacers at both ends of the capsule. The hot piston-in method was used to pressurize the assembly. Pressure was regulated automatically during the experiments. 18% friction correction for the talc-Pyrex assembly at Bayreuth and 3% friction correction for the NaCl + Pyrex assembly at Guangzhou were applied to the nominal pressure based a bracketing of the quartz–coesite transition at 790 °C with the data of Bose and Ganguly (1995) as reference. Temperature was measured and controlled with $Pt/Pt_{90}Rh_{10}$ thermocouples (S-type) connected to a Eurotherm controller, with a variation within ±2 °C for the nominal temperature during experiment and an estimated uncertainty of ±15 °C due to a temperature gradient over the capsule. For each experiment, the charge was initially heated to a temperature 100 °C above the target temperature and held for 30 min, and then cooled to the final temperature within 20 min to promote the growth of crystals. The charge was quenched by switching off the electrical power. After each experiment the capsule was took out from the assembly inside the pressure vessel and then mounted in epoxy and polished for optical observations and chemical analyses.

2.4. EMP analysis

Major elements and CuO (wt.%) in minerals and quenched glasses were measured with the JEOL JXA-8100 microprobe at Guangzhou Institute of Geochemistry or with the JEOL JXA-8200 microprobe at Bayerisches Geoinstitut. The following conditions were used for measurements of all the standardizations and samples. A 1 μm beam was used for analysis of the minerals and 20 μm diameter beams were used for analysis of the quenched glasses except for run Cu-5#, where 5 μm was used due to crystals in the glass of this run present everywhere. The accelerating voltage was 15 kV at currents of 20 nA for all elements in minerals and 20 nA for Cu and 10 nA for other elements in quenched glasses, with counting times of 20 s on the peaks for all elements except Na, K and Cu, where 10 s on the peaks for Na and K and 40 s on the peak for Cu were used. The analyses were performed in wavelength-dispersive mode, and a PAP matrix correction was applied to the raw data. The standards used were andradite (Si), $MnTiO_3$ (Ti), spinel (Al), metal Fe (Fe), $MnTiO_3$ (Mn), forsterite (Mg), wollastonite (Ca), albite (Na), orthoclase (K), Gallium phosphite (P), metal Ni (Ni), metal Cr (Cr) and metal Cu (Cu). The detection limit for Cu was ~350 ppm. For comparison, olivine and quenched glasses from run Cu-46# and run Cu-30# were analyzed with both the JEOL JXA-8100 microprobe at Guangzhou Institute of Geochemistry and the JEOL JXA-8200 microprobe at Bayerisches Geoinstitut. The results revealed very good agreement between the measurements (major elements and CuO) of both the machines (Table S2).

2.5. LA-ICP-MS analysis

Cu and Rb (ppm) in minerals and quenched glasses were determined with the LA-ICP-MS at Bayerisches Geoinstitut or at Guangzhou Institute of Geochemistry. The former uses a Geolas M 193 nm ArF excimer laser attached to an Elan DRC-e ICP-MS. The latter uses a Resonetic 193 nm ArF excimer laser attached to an Agilent 7500a ICP-MS. During the analyses, major elements ^{23}Na, ^{25}Mg, ^{28}Si, ^{27}Al, ^{39}K, ^{43}Ca, ^{49}Ti, ^{55}Mn and ^{57}Fe were also monitored. Operations of the laser were: 5–10 Hz frequencies, 80 mJ energy and 20–80 μm spot sizes mostly with 30 μm. The sample chamber was flushed with He at a rate of 0.4 L/min, and H_2 at a rate of 5 ml/min was added to the He-carrier gas flow to increase the sensitivity of Cu. ^{65}Cu and ^{85}Rb were the chosen isotopes for Cu and Rb analyses. Peak counting times of 30 ms for Cu and 10 ms for Rb were used. NIST SRM 610 glass was used as the external standard. Si (or Ca or Al) determined by electron microprobe was used as the internal standard. The reproducibility (1σ) of the measured Cu and Rb in the SRM 610 standard is <10%.

Analytical points for quenched glasses were positioned in areas without tiny minerals and water bubbles, whereas analytical points for minerals were positioned in the rims. The reliability of mineral analyses was monitored by the behavior of Rb. Rubidium has extremely low partition coefficients (<0.04) between mantle minerals (olivine, opx, cpx, spinel and garnet) and basaltic–basaltic andesite liquids (Rollinson, 1993), hence contaminations from silicate melt can easily be recognized by means of elevated Rb signals. As shown in Fig. 2, the signals of Rb for olivine, opx and cpx from run Komatiite-L1 indicate no melt inclusions within the analyzed area and no analytical contamination of the glass; whereas the signals of Cu for these minerals indicate the homogeneity of Cu and the absence of any melt inclusion and Cu-bearing nugget.

Cu and Rb analyses of olivines and quenched glasses from Cu-46# and Cu-30# (Table S2) determined by the LA-ICP-MS at Guangzhou Institute of Geochemistry and the one at Bayerisches Geoinstitut were compared to test whether there is a system error between the two instruments. The results show excellent (<10 rel%) agreement between them. Analyses for all the run products show that the Cu concentration is higher than 10 ppm in minerals (except the diopside in run Cu-35#, which contains only 4.1 ppm Cu) and higher than 100 ppm in melts. The relatively high Cu concentrations in our run products allow obtaining precise and reliable LA-ICP-MS analyses for this element.

2.6. Comparison between Cu analyses by EMP and LA-ICP-MS

All the EMP and LA-ICP-MS analyses are listed in Tables 3–7. The concentrations of Cu in minerals and quenched glasses determined by LA-ICP-MS and determined by EMP were compared. As shown in Fig. 3, the EMP method overestimates the concentration of Cu when

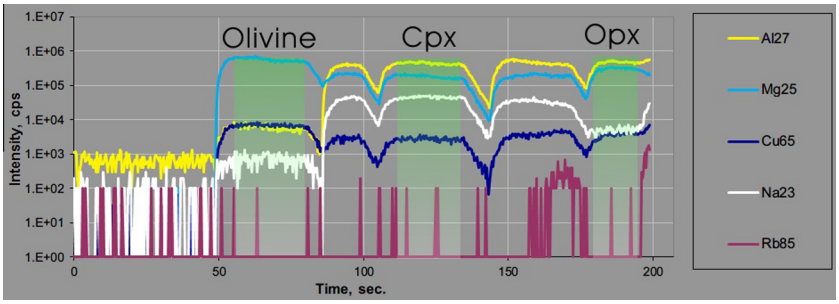

Fig. 2. Time-resolved LA-ICP-MS spectra of olivine, clinopyroxene and orthopyroxene from run Komatiite-L1. The chosen integration intervals show relatively constant signal intensities and no elevated Rb, suggesting that there is no contamination by co-ablated glass.

Cu concentrations are lower than ~400 ppm. Above 400 ppm, both the methods obtained identical results within error (only two points deviate very slightly from the diagonal line in Fig. 3), which is consistent with the results of Fellows and Canil (2012). For the calculations of partition coefficients, we used the LA-ICP-MS results for all the glasses and for the crystals larger than 20 μm. Some crystals are too small to be analyzed by LA-ICP-MS. In this case, the EMP values were also used if the Cu concentrations in crystals are above 400 ppm.

3. RESULTS

3.1. General

Twenty-one successful experiments (Table 2: 9 Komatiite runs, 7 MORB runs and 5 $Di_{70}An_{30}$ runs) produced target minerals and quenched silicate melts suitable for major and trace element analyses. The nine Komatiite experiments were conducted at 1.0 GPa and 1250–1300 °C (Table 2). These experiments produced olivine, opx, cpx and spinel. Olivine, cpx and spinel as subdural crystals were present in all the Komatiite runs but opx was produced only in three runs. The crystals of olivine and opx are relatively large, up to 200 μm and mostly >30 μm (Fig. 4) and can be easily analyzed by both EMP and LA-ICP-MS, whereas the crystals of spinel are small (<10 μm) and were analyzed only by EMP. Only two Komatiite runs contain cpx crystals large enough for LA-ICP-MS analysis although this phase was present in several runs. The acicular or dendritic appearances of this phase in runs Cu-31# and Cu-55# suggest that they were quenched products.

The seven MORB experiments were performed at 1.0–3.5 GPa and 1150–1250 °C (Table 2). Cpx was present in all these runs, whereas garnet was produced only in two runs at 3.5 GPa and 1200 °C (MORB-L5 and MORB-L6). Spinel and plagioclase were saturated at 1.0 GPa and 1150 °C in run Cu-6# and run Cu-41, respectively. The crystals of cpx, garnet and plagioclase are large, typically ranging from 20 to 300 μm, 30 to 80 μm and 20 to 250 μm, respectively, whereas the crystals of spinel were also up to 25 μm, larger than those produced in the Komatiite experiments.

The five $Di_{70}An_{30}$ experiments were conducted at 1.0 GPa and 1215–1240 °C (Table 2). All these experiments only produced nearly Fe-free cpx (diopside) with grains large (up to 200 μm) enough for LA-ICP-MS analysis.

Fe loss in each run of all the Fe-bearing experiments (Komatiite and MORB compositions) was estimated by mass balance and is also reported in Table 2. The extent of Fe loss significantly depends on fO_2 and to a smaller extent on temperature, H_2O content and experimental duration. For the Komatiite experiments, the Fe loss at $fO_2 > FMQ + 3$ is less than 15%, whereas at $fO_2 \leqslant FMQ + 1.2$ is larger than 60% and up to 88%. For the MORB experiments, Fe loss in the run buffered by HM is 13%, whereas in the two runs buffered by NNO is 76% and 90%, respectively. These results demonstrate that Fe loss at relatively reduced conditions is a severe problem in the experiments with Pt (or Pt-rich) capsules.

3.2. Melt compositions

The compositions of hydrous melts are reported in Table 3 and the corresponding anhydrous compositions (EMP analyses normalized to 100%) are reported in Table S3. According to the difference of EMP analytical total to 100%, the estimated amounts of dissolved water range from 3.5 to 11.5 wt.% with mostly lower than 10 wt.%. It should be noted that the estimated H_2O contents in most quenched melts are higher than expected from the H_2O contents added to the starting compositions. This is due to H_2 diffusion from the buffer materials through the capsule wall into the samples and then H_2 combining with O_2 to form H_2O dissolved in the melts. Melt compositions are controlled by the starting composition and crystalline phase assemblage and compositions. For the Komatiite experiments, the anhydrous melt compositions (45.5–52.0 wt.% SiO_2) are komatiitic to basaltic. Compared to natural MORBs, they are generally richer in MgO but poorer in SiO_2 and Na_2O. Their Mg# values range from 45 to 89 and are mostly higher than 57 of the average MORB (Hofmann, 1988). The very high melt Mg# values 89, 84 and 87 for runs Cu-50#, Komatiite-L4 and Komatiite-L2 are a result of Fe loss (Table 2). For the MORB experiments, the anhydrous melt compositions (51.3–58.0 wt.% SiO_2) are basaltic to andesitic with Mg# mostly ranging from 38 to

Table 3
Compositions of hydrous silicate melts.

Run No.	Cu-50#	Cu-46#	Cu-31#	Cu-5#	Cu-30#	Cu-55#	Komatiite-L4	Komatiite-L2	Komatiite-L1	Cu-41#	
EMP (wt.%)											
n	13	8	14	10	11	18	16	15	12	15	
SiO_2	48.36(0.64)	44.22(0.30)	42.65(0.50)	46.27(1.31)	43.65(0.41)	44.01(0.14)	46.77(0.17)	51.10(0.77)	43.98(0.20)	48.72(0.34)	
TiO_2	0.28(0.05)	0.54(0.02)	0.48(0.02)	0.74(0.06)	0.39(0.05)	0.49(0.04)	0.76(0.03)	0.78(0.04)	0.69(0.03)	1.37(0.09)	
Al_2O_3	14.68(0.27)	11.39(0.16)	9.72(0.14)	14.82(1.07)	9.51(0.43)	10.26(0.09)	15.77(0.11)	16.27(0.65)	14.03(0.11)	15.22(0.25)	
FeO	2.99(0.18)	11.37(0.15)	9.57(0.23)	9.44(1.86)	9.62(0.35)	9.50(0.12)	3.98(0.24)	1.14(0.11)	10.62(0.11)	10.84(0.14)	
MnO	0.10(0.02)	0.17(0.03)	0.18(0.02)	0.18(0.03)	0.14(0.03)	0.22(0.04)	0.18(0.03)	0.17(0.02)	0.17(0.03)	0.02(0.01)	
MgO	13.41(0.45)	15.15(0.21)	20.57(0.27)	4.23(1.02)	18.76(0.55)	20.68(0.19)	11.48(0.17)	4.30(1.10)	10.76(0.08)	5.05(0.09)	
CaO	12.89(0.26)	9.72(0.11)	8.34(0.12)	11.24(0.38)	8.86(0.10)	8.74(0.06)	11.50(0.09)	13.87(0.40)	11.15(0.10)	9.35(0.06)	
Na_2O[b]	1.10(0.04)	0.89(0.05)	0.74(0.04)	0.55(0.15)	0.78(0.08)	0.75(0.03)	1.27(0.04)	0.85(0.21)	1.11(0.04)	3.22(0.09)	
K_2O	0.10(0.02)	0.07(0.01)	0.06(0.01)	0.08(0.02)	0.07(0.01)	0.06(0.01)	0.10(0.01)	0.09(0.02)	0.09(0.01)	0.29(0.02)	
P_2O_5	0.12(0.02)	0.07(0.01)	0.06(0.02)	0.12(0.05)	0.05(0.02)	0.06(0.02)	0.11(0.02)	0.15(0.05)	0.11(0.04)	0.23(0.02)	
NiO	0.02(0.02)	0.14(0.04)	0.09(0.04)	0.03(0.03)	0.15(0.06)	0.09(0.02)	0.02(0.02)	0.01(0.02)	0.07(0.04)	0.02(0.01)	
Cr_2O_3	0.19(0.04)	0.16(0.02)	0.23(0.04)	0.09(0.03)	0.21(0.03)	0.31(0.02)	0.10(0.03)	0.17(0.04)	0.03(0.02)	0.03(0.01)	
CuO	0.04(0.03)	1.54(0.29)	1.02(0.06)	1.17(0.18)	0.82(0.11)	1.30(0.06)	0.11(0.02)	0.07(0.03)	0.63(0.04)	0.19(0.05)	
Total	94.28(0.62)	96.23(0.28)	93.71(0.37)	88.95(0.99)	93.02(0.99)	96.47(0.31)	92.15(0.19)	88.97(0.46)	93.45(0.33)	94.54(0.43)	
H_2O [c]	5.7	3.6	7.3	10.8	7.1	3.5	7.9	11.0	6.6	5.2	
Mg#	88.99	70.58	79.46	44.61	77.83	79.66	83.85	87.18	64.58	45.61	
LA-ICP-MS											
n	7	2	2	–	3	7	4	6	2	2	
Cu (ppm)	281(8)	13,271(2214)	8487(17)	n.a.	5848(40)	13,034(559)	866(41)	783(187)	5125(655)	1497(191)	
Rb (ppm)	206(12)	124(4)	94(0)	n.a.	120(1)	168(6)	215(4)	219(22)	282(1)	22(1)	

Run No.	Cu-6#	MORB-L2	MORB-L1[a]	MORB-L3	MORB-L5	MORB-L6	Cu-35#	Cu-47#	Cu-52#	Cu-43#	Cu-48#
EMP (wt.%)											
n	30	10	–	10	8	10	20	10	10	25	10
SiO_2	49.43(0.29)	49.49(0.16)	53.00(0.00)	52.13(0.23)	50.42(0.37)	50.89(0.46)	49.47(0.40)	47.26(0.31)	46.53(0.24)	45.63(0.55)	47.10(0.18)
TiO_2	1.03(0.07)	1.84(0.05)	1.67(0.03)	2.11(0.05)	2.45(0.06)	2.30(0.16)	0.02(0.02)	0.03(0.03)	0.03(0.01)	0.03(0.02)	0.03(0.02)
Al_2O_3	15.59(0.11)	16.62(0.08)	14.79(0.09)	17.01(0.08)	13.68(0.14)	13.92(0.12)	16.83(0.34)	13.51(0.26)	15.00(0.13)	15.93(0.58)	12.45(0.15)
FeO	8.23(0.17)	2.03(0.03)	9.44(0.36)	0.83(0.04)	8.29(0.19)	7.24(0.22)	0.02(0.02)	0.02(0.02)	0.14(0.03)	0.11(0.02)	0.13(0.02)
MnO	0.02(0.01)	0.02(0.02)	0.01(0.00)	0.01(0.01)	–	–	0.02(0.02)	0.01(0.01)	0.02(0.02)	0.02(0.01)	0.02(0.01)
MgO	5.39(0.09)	5.62(0.05)	6.11(0.43)	4.85(0.05)	2.81(0.08)	2.79(0.07)	4.91(0.24)	7.55(0.16)	6.10(0.13)	6.02(0.24)	9.07(0.11)
CaO	8.98(0.13)	9.32(0.09)	10.41(0.72)	8.96(0.12)	7.95(0.07)	7.64(0.10)	23.53(0.17)	21.39(0.17)	21.43(0.17)	23.36(0.11)	22.50(0.15)
Na_2O[b]	3.18(0.11)	2.88(0.07)	3.09(0.04)	3.09(0.09)	3.74(0.23)	4.15(0.28)	0.12(0.02)	0.76(0.04)	0.07(0.02)	0.11(0.02)	0.10(0.02)
K_2O	0.26(0.02)	0.29(0.02)	0.31(0.03)	0.30(0.02)	0.39(0.01)	0.39(0.01)	0.10(0.01)	0.12(0.01)	0.05(0.01)	0.06(0.01)	0.06(0.01)
P_2O_5	0.30(0.02)	0.34(0.03)	0.34(0.00)	0.44(0.03)	0.50(0.02)	0.50(0.03)	0.02(0.01)	0.02(0.01)	0.02(0.01)	0.02(0.01)	0.02(0.01)
NiO	0.02(0.01)	0.02(0.02)	–	0.01(0.01)	0.02(0.02)	0.03(0.02)	0.03(0.02)	0.01(0.00)	0.02(0.02)	0.04(0.04)	0.02(0.01)
Cr_2O_3	0.03(0.01)	0.01(0.02)	–	0.01(0.01)	0.02(0.02)	0.02(0.02)	0.02(0.01)	0.02(0.02)	0.03(0.02)	0.02(0.02)	0.03(0.02)
CuO	0.51(0.04)	0.05(0.02)	0.61(0.03)	0.07(0.02)	0.30(0.02)	0.34(0.03)	0.03(0.01)	0.07(0.04)	0.47(0.04)	0.48(0.04)	0.69(0.04)
Total	92.92(0.50)	88.52(0.34)	99.17(0.00)	89.84(0.32)	87.66(0.61)	86.89(0.71)	95.06(0.54)	90.74(0.42)	89.88(0.46)	91.78(0.40)	92.18(0.33)
H_2O [c]	7.1	11.5	–	10.2	9.6	10.0	4.9	9.3	10.1	8.2	7.8
Mg#	54.09	83.29	53.80	91.37	37.91	40.91	–	–	–	–	–

(*continued on next page*)

Table 3 (*continued*)

Run No.	Cu-6#	MORB-L2	MORB-L1[a]	MORB-L3	MORB-L5	MORB-L6	Cu-35#	Cu-47#	Cu-52#	Cu-43#	Cu-48#
LA-ICP-MS											
n	4	3	2	3	3	3	6	6	7	6	6
Cu (ppm)	4885(76)	420(9)	4906(198)	524(10)	3574(320)	3817(242)	107(2)	610(21)	4777(228)	5143(71)	6966(123)
Rb (ppm)	21(2)	153(2)	147(14)	185(3)	238(8)	245(16)	99(1)	61(3)	76(3)	80(3)	52(1)

Note: n: number of analyses. Number in bracket corresponds to 1σ standard deviation. n.a. = not analyzed. Mg# = molar MgO/(MgO + FeO) × 100.

[a] Major and trace elements of silicate melt in MORB-L1 measured by LA-ICP-MS.

[b] The melts produced in MORB-L5 and MORB-L6 have severe Na loss during the EMP analysis. The Na_2O contents and analytical totals for the two melts are the values calibrated by mass balance calculation.

[c] H_2O (wt%) in the melt was estimated by the difference of EMPA total to 100%.

65, which are comparable to the Mg# values in normal basalts and andesites. Two very high Mg# values 83 (MORB-L2) and 91 (MORM-L3) are also due to the significant Fe loss in the two runs (Table 2). For the $Di_{70}An_{30}$ experiments, the anhydrous melt compositions (49.7–52.1 wt.% SiO_2) are basaltic except that they are nearly Fe-, Na- and K-free and higher in CaO compared to normal basalts.

3.3. fO_2 and Cu solubility and valence states in melts

Fourteen experiments in this study were buffered by graphite, FMQ, NNO, MnMnO or HM to impose fO_2 from ~FMQ − 2 to ~FMQ + 5 on the samples. The calculated theoretical values of fO_2 at experimental P-T conditions for these buffers relative to FMQ are given in Table 2. Previous experiments (Ripley and Brophy, 1995; Holzheid and Lodders, 2001; Ripley et al., 2002) have well demonstrated that the solubility of Cu in silicate melts significantly increases with increasing fO_2. The Cu apparent solubility (Cu in melt) data from our experiments (Table 2) also show the same variation trend: Cu concentrations in melts increase from <300 ppm for the graphite buffers to 420–783 ppm for the NNO buffers and then to >4000 ppm for the MnMnO and HM buffers. These indicate that a relative fO_2 scale was established in our experiments. It should be noted that the FMQ buffers in runs Cu-30#, Cu-43# and Cu-52# failed. In these three runs, we found only magnetite and quartz but no fayalite in the buffer materials after the experiments. This is in agreement with the fact that fayalite in the FMQ buffer material is not stable at temperatures higher than 1200 °C (Hsu, 1967). Although the exact fO_2 values are not known in the three runs, the high apparent solubility values of Cu (4777–6373 ppm) in the corresponding melts suggest that they have high fO_2 values, even higher than the NNO buffer. Seven experiments were not buffered by any externally imposed oxygen buffer. The Cu apparent solubility values for these experiments are in the wide range of 610–13,271 ppm, indicating large variations of fO_2 among these experiments.

Run products in all the nine Komatiite experiments were saturated with olivine and spinel, which made it possible to calculate the true fO_2 values for these runs with the olivine-opx-spinel oxygen geobarometer (Ballhaus et al., 1990, 1991). For this oxygen geobarometer, the chemical composition of opx is not required as an input parameter. Furthermore, in the opx-absent melts, the barometer also gives reasonable results and the correction required rarely exceeds ~0.2 log units (Ballhaus et al., 1991). Using this oxygen geobarometer, we have estimated the fO_2 values of these experiments (Table 2). The estimated fO_2 in the runs with external HM, MnMnO and graphite buffers are 0.1–0.5 log units lower than their corresponding theoretical values. For piston cylinder experiments with a double-capsule technique, the fO_2 attained in the sample during the experiment would be a little lower than the externally imposed oxygen buffer because the water activity in the silicate melt was less than unity (Li and Audétat, 2012). The estimated value for the run (Komatiite-L2) with the NNO buffer is 0.5 log units higher than its corresponding theoretical value. The reason for this overestimation is unclear.

Table 4
Compositions of olivines.

Run No.	Cu-50#	Cu-46#	Cu-31#	Cu-5#	Cu-30#	Cu-55#	Komatiite-L4	Komatiite-L2	Komatiite-L1
EMP (wt.%)									
n	18	31	10	60	9	17	13	63	20
SiO_2	40.69(0.22)	40.79(0.26)	40.76(0.42)	40.38(0.47)	40.88(0.18)	40.44(0.18)	40.32(0.22)	40.95(0.19)	40.72(2.61)
TiO_2	0.01(0.02)	0.03(0.02)	0.02(0.01)	0.03(0.02)	0.07(0.00)	0.01(0.01)	0.02(0.01)	0.02(0.02)	0.02(0.03)
Al_2O_3	0.11(0.13)	0.11(0.09)	0.09(0.01)	0.05(0.02)	0.06(0.01)	0.10(0.03)	0.04(0.02)	0.04(0.02)	0.32(1.20)
FeO	5.11(0.51)	6.57(0.18)	4.90(0.21)	7.72(0.37)	6.42(0.10)	4.56(0.16)	5.22(0.92)	1.85(0.27)	8.37(0.23)
MnO	0.18(0.02)	0.10(0.02)	0.08(0.02)	0.11(0.03)	0.10(0.03)	0.12(0.02)	0.18(0.03)	0.15(0.03)	0.16(0.03)
MgO	54.01(0.48)	49.32(0.43)	50.12(0.50)	49.95(0.62)	49.07(0.12)	53.88(0.25)	53.34(0.71)	55.93(0.37)	50.27(4.30)
CaO	0.26(0.02)	0.23(0.07)	0.18(0.01)	0.14(0.02)	0.17(0.01)	0.20(0.02)	0.19(0.02)	0.17(0.03)	0.26(0.31)
Na_2O	–	0.02(0.01)	0.04(0.02)	0.03(0.01)	0.04(0.02)	0.01(0.02)	0.01(0.01)	0.01(0.01)	0.01(0.01)
K_2O	–	0.01(0.01)	0.01(0.01)	0.01(0.01)	0.01(0.01)	–	0.01(0.00)	–	–
P_2O_5	0.02(0.02)	0.02(0.01)	0.01(0.01)	0.01(0.01)	0.02(0.01)	0.01(0.01)	0.01(0.01)	0.02(0.02)	0.01(0.01)
NiO	0.06(0.04)	1.59(0.09)	1.34(0.26)	0.62(0.06)	1.26(0.12)	0.36(0.04)	0.12(0.07)	0.05(0.03)	0.66(0.11)
Cr_2O_3	0.19(0.12)	0.08(0.03)	0.10(0.04)	0.04(0.02)	0.09(0.03)	0.12(0.03)	0.07(0.02)	0.13(0.07)	0.03(0.03)
CuO	0.01(0.01)	0.15(0.03)	0.12(0.02)	0.10(0.03)	0.07(0.02)	0.18(0.04)	0.02(0.02)	0.03(0.02)	0.09(0.02)
Total	100.66(0.30)	98.97(0.66)	97.73(0.39)	99.15(0.88)	98.19(0.20)	99.99(0.37)	99.56(0.37)	99.35(0.40)	100.90(0.48)
Mg#	95.0	93.1	94.8	92.0	93.2	95.5	94.8	98.2	91.5
$K_D^{Fe\text{-}Mg}$	0.42	0.18	0.21	0.07	0.26	0.18	0.28	0.12	0.17
LA-ICP-MS									
n	7	5	3	2	6	3	3	4	3
Cu (ppm)	15(1)	1426(47)	827(34)	690(32)	631(89)	1326(33)	46(6)	30(2)	733(16)
Rb (ppm)	BDL	BDL	0.1(0.1)	BDL	BDL	BDL	BDL	BDL	BDL

Note: n: number of analyses. BDL = below detection limit. Number in bracket corresponds to 1σ standard deviation. Mg# = molar MgO/(MgO + FeO) × 100. $K_D^{Fe-Mg} = [X_{Fe}^{mineral} * X_{Mg}^{liq}]/[X_{Mg}^{mineral} * X_{Fe}^{liq}]$.

With the estimated fO_2 values and the corresponding melt Cu solubilities at 1300 and 1250 °C, the Cu apparent solubilities in melts increase linearly with increasing fO_2 at the two temperatures, as shown in Fig. 5. The valence state of dissolved Cu may be estimated using these apparent solubility data and the reaction (Ripley and Brophy, 1995): $Cu^{metal} + n/2\ O_2 = CuO_n^{melt}$, where $\log$Cu solubility (ppm) $= n/2\ \log fO_2 + \log C$. The value of n may be determined from a plot of $\log$Cu (ppm) vs. $\log fO_2$. A slope of 0.5 ($n = 1$) indicates an oxidation state of 2+, whereas a slope of 0.25 ($n = 0.5$) suggests an oxidation state of 1+. At 1300 °C, our data yield slopes of 0.17 ± 0.09 at $fO_2 \leqslant FMQ + 1.2$ and 0.44 ± 0.15 at $fO_2 \geqslant FMQ + 1.2$. At 1250 °C and $fO_2 \geqslant FMQ + 1.2$, the data yield a slope of 0.43 ± 0.39. The change of slope caused by the change of fO_2 should indicate a change of Cu valence state in the melts. At $fO_2 \leqslant FMQ + 1.2$, a formal valence of 0.68 ± 0.34 for Cu is obtained from the 1300 °C data. This suggests that monovalent Cu at these low fO_2 conditions was dominant, consistent with the results at reduced conditions of Ripley and Brophy (1995) and Holzheid and Lodders (2001). At $fO_2 \geqslant FMQ + 1.2$, a formal valence state of $\sim 1.76 \pm 0.58$ is obtained from the 1300 °C data, which could suggest a substantial contribution by divalent Cu added to the monovalent Cu in the melts at the high fO_2 conditions.

3.4. Mineral compositions

Compositions of olivines are reported in Table 4. All the olivines were produced in the Komatiite experiments. Olivines from a single run is compositionally homogeneous with very small standard deviations for all the analyzed elements. Analyses from the nine runs show that olivines contain 40.32–40.95% SiO_2, 49.07–54.01% MgO and 4.56–8.37% FeO and minor concentrations of MnO, CaO, NiO and Cr_2O_3, showing small compositional variations except for FeO. All the olivines are Mg-rich with Mg# [molar MgO/(MgO + TFeO)] ranging from 92 to 98, a little higher than, but significantly overlapping the 90–95 Mg# in the olivines equilibrated with Komatiitic melts (Walter, 1998). The ol/melt Fe–Mg exchange distribution coefficient $[K_D^{Fe-Mg} = (X_{Fe}^{ol} \cdot X_{Mg}^{liq})/(X_{Mg}^{ol} \cdot X_{Fe}^{liq})]$ is in the range of 0.07–0.42 (Table 4). Except the highest value 0.42 that is at the graphite buffer, all of them (0.07–0.28) are lower than the average ol/melt K_{Fe-Mg} value 0.35 ± 0.03 in the peridotite melting with the graphite buffer (Walter, 1998).

Whether or not the generally higher Mg# and the lower ol/melt K_D^{Fe-Mg} values in this study imply Fe–Mg exchange disequilibrium should be assessed and discussed. In principle, olivine Mg# and ol/melt K_D^{Fe-Mg} are significantly related to Fe^{2+}/Mg ratio in the melt, which is controlled by the imposed fO_2 and total Fe in the experimental charge. In this study, the Komatiite experiments at $fO_2 > FMQ + 3$ have slight Fe loss (<15%, Table 2), but the Fe^{2+}/Mg ratios in the corresponding melts are low due to the high fO_2, while those at $fO_2 \leqslant FMQ + 1.2$ have significant Fe loss and thus low total Fe, which also resulted in low Fe^{2+}/Mg ratios in the corresponding melts. Hence, olivines crystallizing from these low Fe/Mg melts have high Mg# and thus low ol/melt K_D^{Fe-Mg}. These explain why the ol/melt K_D^{Fe-Mg} values in this study are generally lower than the average value 0.35 ± 0.03 in the peridotite melting (Walter, 1998) and why these olivines are generally higher in Mg#. However, this does not imply that ol/melt Fe–Mg exchange reached equilibrium in our experiments. A more reasonable assessment should

Table 5
Compositions of pyroxenes.

Run No.	Cu-50#	Komatiite-L4	Komatiite-L1	Komatiite-L4	Komatiite-L1	Cu-41#	Cu-6#
Phase	Opx	Opx	OPx	Cpx	Cpx	Cpx	Cpx
EMP (wt.%)							
n	18	12	18	10	10	24	7
SiO_2	55.11(0.80)	53.71(0.48)	52.60(0.72)	50.71(0.36)	48.83(1.42)	49.55(0.87)	45.09(0.99)
TiO_2	0.05(0.03)	0.09(0.02)	0.07(0.02)	0.18(0.04)	0.18(0.10)	0.71(0.14)	0.72(0.18)
Al_2O_3	3.38(1.05)	3.74(0.32)	4.22(0.69)	4.44(0.52)	5.57(1.30)	6.37(1.12)	8.84(1.31)
FeO	4.43(0.86)	4.37(1.09)	7.47(0.44)	3.33(0.52)	6.64(0.63)	9.00(0.61)	8.61(0.68)
MnO	0.09(0.02)	0.17(0.03)	0.17(0.03)	0.15(0.04)	0.14(0.06)	0.02(0.01)	0.03(0.01)
MgO	32.18(0.58)	33.60(1.14)	32.52(0.44)	19.15(0.47)	17.61(1.19)	13.97(0.91)	11.65(0.81)
CaO	2.13(0.18)	1.88(0.21)	1.80(0.14)	18.88(1.03)	19.15(0.86)	19.42(0.84)	22.05(0.50)
Na_2O	0.05(0.02)	0.03(0.01)	0.02(0.01)	0.26(0.03)	0.26(0.04)	0.59(0.06)	1.03(0.13)
K_2O	0.01(0.00)	0.01(0.01)	–	0.01(0.01)	0.01(0.01)	0.02(0.02)	0.02(0.01)
P_2O_5	0.01(0.01)	0.01(0.02)	–	0.02(0.02)	0.01(0.03)	0.03(0.01)	0.04(0.01)
NiO	0.03(0.02)	0.04(0.03)	0.20(0.03)	0.04(0.03)	0.12(0.04)	0.05(0.03)	0.06(0.05)
Cr_2O_3	1.05(0.26)	1.10(0.11)	0.35(0.10)	1.18(0.13)	0.17(0.11)	0.08(0.05)	0.02(0.01)
CuO	0.02(0.02)	0.02(0.02)	0.05(0.04)	0.02(0.03)	0.04(0.04)	0.04(0.02)	0.06(0.03)
Total	98.51(0.65)	98.78(0.40)	99.48(0.25)	98.37(0.32)	98.73(0.66)	99.78(0.33)	98.18(0.74)
Wo	4.2	3.8	3.7	40.7	42.9	43.6	56.8
En	88.9	93.6	92.5	57.4	54.9	43.6	41.8
Fs	6.9	2.6	3.8	1.8	2.2	12.8	1.4
$K_D^{Fe\text{-}Mg}$	0.62	0.38	0.23	0.50	0.38	0.30	0.48
Mg#	92.9	93.3	88.7	91.2	82.7	73.6	70.9
LA-ICP-MS n	14	5	2	4	4	6	–
Cu (ppm)	10(1)	34(6)	484(2)	52(7)	338(43)	57(5)	n.a.
Rb (ppm)	BDL	BDL	BDL	BDL	BDL	BDL	n.a.

Run No.	MORB-L2	MORB-L1	MORB-L3	MORB-L5	MORB-L6	Cu-35#	Cu-47#	Cu-52#	Cu-43#	Cu-48#
Phase	Cpx	Cpx	Cpx	Cpx	Cpx	Di	Di	Di	Di	Di
EMP (wt.%)										
n	12	10	10	10	13	22	11	15	23	6
SiO_2	50.27(0.31)	47.59(0.56)	50.37(0.27)	48.09(0.72)	48.39(0.55)	51.33(1.17)	53.58(0.66)	52.07(1.25)	52.38(0.51)	52.77(0.51)
TiO_2	0.51(0.07)	0.42(0.09)	0.63(0.07)	0.50(0.08)	0.54(0.11)	0.02(0.01)	0.02(0.01)	0.03(0.02)	0.03(0.02)	0.03(0.02)
Al_2O_3	8.56(0.83)	10.00(0.91)	11.13(0.38)	11.07(0.37)	10.85(0.48)	5.17(1.75)	2.05(0.67)	5.04(1.72)	3.22(0.48)	2.59(0.37)
FeO	3.90(1.34)	7.62(0.33)	1.55(0.82)	8.92(0.42)	8.38(0.48)	0.02(0.01)	0.02(0.01)	0.11(0.04)	0.06(0.02)	0.04(0.01)
MnO	0.01(0.01)	0.01(0.01)	0.01(0.02)	0.01(0.00)	–	0.02(0.01)	0.02(0.01)	0.02(0.01)	0.02(0.02)	0.02(0.00)
MgO	13.86(0.40)	12.08(0.57)	13.25(0.34)	9.36(0.33)	9.31(0.20)	15.88(0.74)	17.13(0.42)	16.36(0.79)	16.59(0.25)	17.19(0.27)
CaO	19.76(0.39)	18.56(0.22)	19.12(0.44)	17.85(0.43)	17.82(0.43)	26.99(0.23)	25.15(0.08)	25.67(0.17)	26.95(0.13)	25.13(0.11)
Na_2O	1.71(0.08)	1.91(0.10)	2.21(0.15)	3.23(0.22)	3.27(0.14)	0.04(0.03)	0.09(0.02)	0.02(0.01)	0.03(0.02)	0.04(0.01)
K_2O	0.01(0.01)	0.01(0.01)	–	–	0.01(0.00)	0.02(0.01)	0.01(0.01)	0.01(0.00)	0.01(0.01)	0.01(0.00)
P_2O_5	0.02(0.02)	0.01(0.01)	0.02(0.02)	0.04(0.02)	0.03(0.00)	0.02(0.01)	0.02(0.01)	0.03(0.01)	0.02(0.01)	0.03(0.01)
NiO	0.02(0.03)	0.03(0.03)	0.01(0.01)	0.02(0.02)	0.03(0.01)	0.06(0.05)	0.01(0.01)	0.04(0.02)	0.05(0.02)	0.02(0.01)
Cr_2O_3	0.03(0.04)	0.06(0.03)	0.06(0.03)	–	–	0.04(0.02)	0.07(0.02)	0.04(0.04)	0.09(0.03)	0.09(0.03)
CuO	0.02(0.01)	0.05(0.02)	0.02(0.02)	0.07(0.02)	0.07(0.02)	0.04(0.02)	0.03(0.02)	0.03(0.02)	0.04(0.02)	0.02(0.01)
Total	98.67(0.24)	98.35(0.17)	98.38(0.15)	99.15(0.95)	98.66(0.55)	99.55(0.40)	98.14(0.56)	99.40(0.41)	99.41(0.44)	97.91(0.55)
Wo	48.1	49.1	49.3	53.3	52.9	55.0	51.3	52.9	53.9	51.2
En	47.0	44.5	47.5	38.8	38.4	45.0	48.6	46.9	46.1	48.7
Fs	4.9	6.4	3.1	7.9	8.7	0.0	0.0	0.2	0.0	0.1
K_D^{Fe-Mg}	0.78	0.22	0.69	0.32	0.35	–	–	–	–	–
Mg#	86.5	74.0	93.9	65.4	66.7	–	–	–	–	–
LA-ICP-MS										
n	2	3	3	3	1	5	8	7	5	6
Cu (ppm)	46(10)	456(38)	70(7)	829(138)	565(0)	4(2)	11(1)	168(17)	203(12)	125(16)
Rb (ppm)	BDL	BDL	BDL	BDL	BDL	0.5(0.3)	BDL	BDL	BDL	BDL

Note: n: number of analyses. n.a. = not analysed. BDL = below detection limit. Number in bracket corresponds to 1σ standard deviation. Mg# = molar MgO/(MgO + FeO) × 100. $K_D^{Fe-Mg} = [X_{Fe}^{mineral} * X_{Mg}^{liq}]/[X_{Mg}^{mineral} * X_{Fe}^{liq}]$. End-members: Wo: wollastonite, En: enstatite, Fs: ferrosilite.

be based on whether the K_D^{Fe-Mg} is a constant at similar fO_2 conditions. For the Komatiite experiments in this study, six runs at $fO_2 > FMQ + 3$ have slight Fe loss (<15%, Table 2) and their ol/melt K_D^{Fe-Mg} (Table 4) range from 0.17 to 0.26 (except run Cu-5#) with the average = 0.20 ± 0.03. The relatively invariable K_D^{Fe-Mg} indicates that olivines from the high fO_2 runs may have approached to Fe–Mg exchange equilibrium. Three runs at $fO_2 \leqslant FMQ + 1.2$ have

Table 6
Compositions of spinels.

Run No.	Cu-50#	Cu-46#	Cu-31#	Cu-5#	Cu-30#	Cu-55#	Komatiite-L4	Komatiite-L2	Komatiite-L1	Cu-6#
Phase	Spl	Spl	Spl	Spl	Spl	Spl	Spl	Spl	Spl	Spl
EMP (wt.%)										
n	4	15	16	15	15	16	18	38	15	10
SiO_2	0.43(0.16)	0.19(0.03)	0.31(0.43)	0.17(0.06)	0.22(0.24)	0.19(0.03)	0.40(0.24)	0.18(0.16)	0.17(0.03)	0.17(0.10)
TiO_2	0.25(0.06)	0.29(0.03)	0.29(0.04)	0.48(0.07)	0.34(0.03)	0.23(0.03)	0.28(0.02)	0.23(0.03)	0.55(0.05)	1.02(0.05)
Al_2O_3	33.00(0.81)	19.84(0.59)	17.06(0.62)	14.00(0.72)	17.79(0.25)	19.97(0.58)	31.69(1.35)	18.39(1.27)	18.05(1.10)	9.53(0.29)
FeO	6.72(0.63)	35.21(0.50)	24.97(0.98)	47.93(3.94)	32.36(0.79)	21.18(0.31)	11.34(0.55)	3.34(0.14)	55.99(0.83)	67.55(2.01)
MnO	0.22(0.03)	0.19(0.03)	0.19(0.03)	0.21(0.03)	0.19(0.03)	0.21(0.03)	0.24(0.03)	0.29(0.03)	0.21(0.03)	0.04(0.03)
MgO	20.72(0.90)	17.24(0.12)	18.08(0.55)	14.26(0.22)	16.95(0.15)	19.57(0.13)	19.59(0.44)	21.64(0.29)	13.68(0.22)	9.69(0.50)
CaO	0.10(0.02)	0.16(0.05)	0.13(0.10)	0.10(0.06)	0.12(0.08)	0.16(0.06)	0.28(0.12)	0.14(0.07)	0.13(0.06)	0.07(0.04)
Na_2O	0.03(0.01)	0.01(0.02)	0.02(0.01)	0.02(0.02)	0.02(0.02)	0.01(0.02)	0.01(0.01)	0.01(0.01)	0.01(0.01)	0.07(0.05)
K_2O	–	–	0.01(0.01)	0.01(0.01)	–	–	0.01(0.01)	0.01(0.01)	–	–
P_2O_5	–	0.01(0.01)	0.01(0.02)	0.01(0.02)	–	0.01(0.02)	0.02(0.02)	0.02(0.02)	0.01(0.01)	0.01(0.01)
NiO	0.03(0.02)	0.86(0.05)	0.35(0.04)	1.20(0.08)	0.59(0.06)	0.33(0.04)	0.12(0.03)	0.04(0.04)	1.04(0.08)	0.12(0.03)
Cr_2O_3	38.47(0.87)	22.86(1.17)	35.73(1.29)	15.82(4.48)	27.98(0.60)	35.70(0.85)	35.92(1.65)	54.91(1.42)	5.79(1.88)	5.62(1.86)
CuO	0.01(0.02)	0.38(0.03)	0.20(0.05)	0.29(0.05)	0.16(0.03)	0.31(0.04)	0.03(0.03)	0.03(0.02)	0.26(0.04)	0.47(0.04)
Total	99.96(0.70)	97.25(0.41)	97.34(0.63)	94.50(0.53)	96.74(0.47)	97.86(0.47)	99.91(0.59)	99.24(0.41)	95.88(0.38)	94.32(1.36)
Fe_2O_3	0.84	30.69	20.56	41.68	27.13	18.52	4.62	1.99	48.09	54.5
Cr#	43.9	43.6	58.4	43.1	51.3	54.5	43.2	66.7	17.7	28.4

Note: n: number of analyses. Number in bracket corresponds to 1σ standard deviation. Cr# = molar $Cr_2O_3/(Cr_2O_3 + Al_2O_3) \times 100$. The Fe_2O_3 content in the spl was calculated assuming perfect stoichiometry.

Table 7
Compositions of garnets and plagioclase.

Run No.	MORB-L5	MORB-L6	Cu-41#
Phase	Grt	Grt	Pl
EMP (wt.%)			
n	14	10	10
SiO_2	38.98(0.62)	39.00(0.97)	51.87(0.35)
TiO_2	0.83(0.45)	1.12(0.45)	0.04(0.02)
Al_2O_3	20.88(0.81)	19.97(1.19)	28.66(0.26)
FeO	14.59(1.54)	15.71(0.87)	0.26(0.07)
MnO	0.04(0.01)	0.03(0.02)	0.03(0.01)
MgO	13.41(1.33)	11.54(0.38)	0.09(0.04)
CaO	10.32(0.53)	11.21(0.58)	13.24(0.22)
Na_2O	0.10(0.04)	0.26(0.27)	4.52(0.10)
K_2O	0.01(0.01)	0.01(0.01)	0.07(0.01)
P_2O_5	0.11(0.05)	0.12(0.02)	0.02(0.01)
NiO	0.03(0.03)	0.02(0.01)	0.04(0.03)
Cr_2O_3	0.04(0.05)	0.02(0.02)	0.01(0.00)
CuO	0.02(0.01)	0.03(0.01)	0.02(0.02)
Total	99.27(0.78)	98.97(0.94)	98.80(0.57)
Mg#	62.3	56.9	–
al	21.5	26.6	An 61.5
py	50.5	43.2	Ab 38.1
gr	23.7	26.3	Or 0.4
an	3.5	2.8	–
ct	0.6	0.9	–
LA-ICP-MS			
n	3	4	5
Cu (ppm)	164(21)	146(12)	35(12)
Rb (ppm)	BDL	BDL	0.6(0.1)

Note: n = number of analyses. BDL = below detection limit. Number in bracket corresponds to the 1σ standard deviation. Mg# = molar MgO/(MgO + FeO) × 100. End-members for garnet: al: almandine, py: pyrope, gr: grossular, an: andradite, ct: Ca-Ti garnet; End-members for feldspar: An: anorthite, Ab: albite, Or: orthoclase.

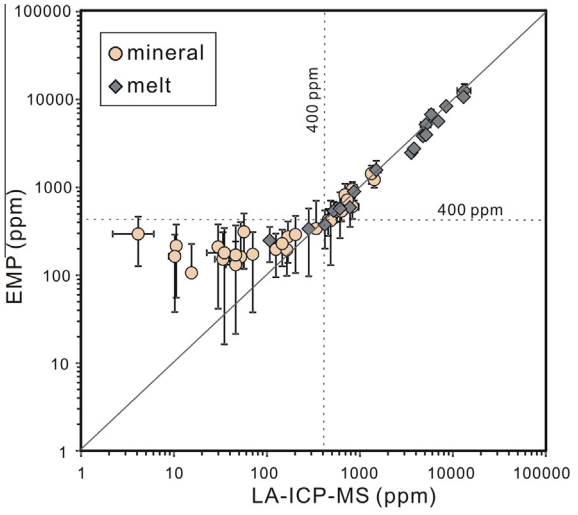

Fig. 3. Comparison of Cu concentrations determined by LA-ICP-MS and EMP, showing that both methods give identical values within errors when Cu concentrations are above 400 ppm (data from Table 3–7, CuO in wt% from the EMP analyses has been changed to Cu in ppm in this figure).

significant Fe loss and the ol/melt K_D^{Fe-Mg} is 0.12, 0.28 and 0.42 (Table 4), respectively, indicating big variations in K_D^{Fe-Mg}. The higher K_D^{Fe-Mg} (0.42) possibly implies that the olivine crystallized before significant Fe loss and the Fe–Mg exchange was not equilibrated in this run, whereas the lower K_D^{Fe-Mg} (0.12 and 0.28) indicates that the olivines crystallized after significant Fe loss. In the latter case, whether the Fe–Mg exchange reached equilibrium is difficult to be assessed clearly because of the different fO_2 and extents of Fe loss in the two runs. Whether or not the Fe loss and Fe–Mg exchange disequilibrium have an effect on the Cu partitioning is of key importance. As will be shown in Section 3.6, the partition

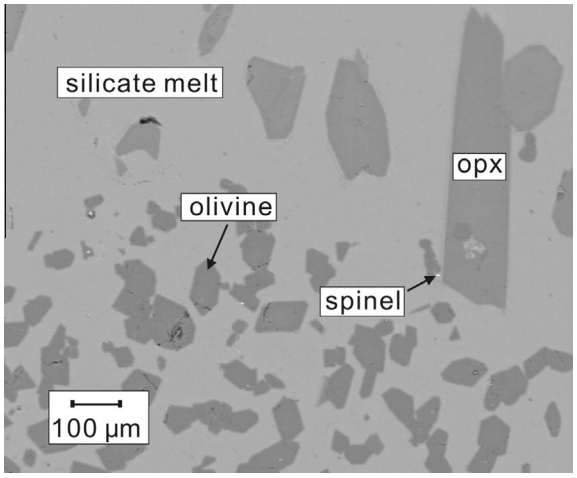

Fig. 4. Representative products in run Cu-50# (Komatiite experiment at 1.0 GPa, 1300 °C and fO_2 buffered by graphite).

coefficients of Cu do not seem to have been affected by the Fe losses.

Compositions of opxs are reported in Table 5. Opx was present in three Komatiite runs (Cu-50#, Komatiite-L1 and Komatiite-L4). They contain 52.60–55.11% SiO_2, 3.74–4.22% Al_2O_3, 32.18–33.60% MgO, 4.37–7.45% FeO and 1.80–2.13% CaO and minor concentrations of MnO, NiO and Cr_2O_3, also showing small compositional variations except for FeO. These opxs are also Mg-rich with Mg# = 89–93, which are in the range of Mg# = 90–94 in the opxs produced in the peridotite melting (Walter, 1998). The opx/melt K_D^{Fe-Mg} values in the three runs are 0.62, 0.38 and 0.23, respectively (Table 5), showing that two of them deviate the average opx/melt K_D^{Fe-Mg} 0.33 ± 0.04 in the peridotite melting (Walter, 1998). The opx with 0.62 K_D^{Fe-Mg} was produced in the run with fO_2 = FMQ − 1.8 and Fe loss = 69% (Table 2) and the Fe–Mg exchange for the opx in this run did not reach equilibrium. The opx with 0.23 K_D^{Fe-Mg} was produced in the run with fO_2 = FMQ + 4.6 and there is no Fe loss in this run (Table 2). This low K_D^{Fe-Mg} does not mean disequilibrium, but is a result of low Fe^{2+}/Mg ratio in the melt at the high fO_2 condition.

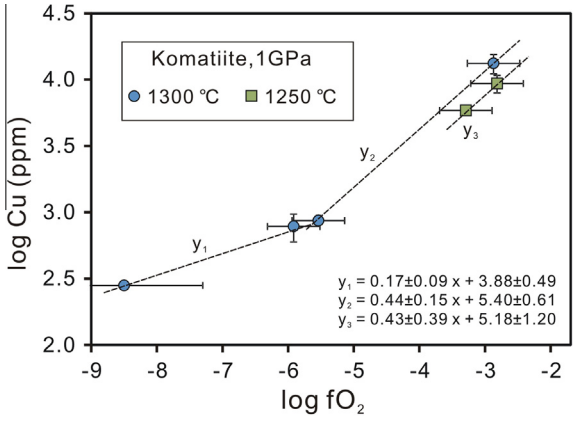

Fig. 5. Cu concentration (apparent solubility) in melt vs. fO_2 for the Komatiite experiments at 1300 and 1250 °C (1.0 GPa). Data are from Table 2 and Table 3 [note: fO_2 (FMQ) = $10^{-6.7}$ at 1.0 GPa and 1300 °C and fO_2 (FMQ) = $10^{-7.2}$ at 1.0 GPa and 1250 °C].

Compositions of cpxs are also reported in Table 5. Cpx was present in two Komatiite runs and in all the MORB and Di_{70}-An_{30} runs. Composition of cpx is also homogeneous in a single run but varies with changes of experimental starting composition and conditions. The cpxs crystallized from the Di-An composition are nearly pure diopsides (only contain SiO_2, CaO, MgO and minor Al_2O_3), whereas those crystallized from the MORB and Komatiite compositions are aluminian-diopsides. The cpx produced in the Komatiite experiments are Mg-high (Mg# = 83–91) and Na-low (0.26 wt.% Na_2O), whereas those from the MORB experiments are relatively MgO-low (Mg# = 67–74) and Na-rich (up to 3.27 wt.% Na_2O), and the Na_2O content in these cpxs increases with increasing pressure. For the Komatiite experiments, the cpx produced in run Komatiite-L4 has cpx/melt K_D^{Fe-Mg} = 0.50, whereas the cpx produced in run Komatiite-L1 has cpx/melt K_D^{Fe-Mg} = 0.38. The former run has significant Fe loss (63%, Table 2) and was possibly in Fe–Mg exchange disequilibrium, whereas the latter run has no Fe loss and was possibly in Fe-Mg exchange equilibrium. For the 7 MORB experiments, the cpx/melt K_D^{Fe-Mg} in the five runs with slight Fe loss (<13%, Table 2) are in the small range of 0.30 to 0.48 (Table 5) with the average = 0.33 ± 0.09, whereas the cpx/melt K_D^{Fe-Mg} in the other two runs with significant Fe loss (76% and 89%) are 0.69 and 0.78. The former are a bit lower than the average cpx/melt K_D^{Fe-Mg} value 0.35 ± 0.05 (Walter, 1998), indicating an approach to Fe–Mg exchange equilibrium. The latter are unusually high compared to that average value and thus are in Fe–Mg exchange disequilibrium.

Compositions of spinels are reported in Table 6. Spinel was present in all the nine Komatiite experiments and in run Cu-6# of the MORB experiments. The spinels produced in the Komatiite experiments contain 5.79–54.91 wt.% Cr_2O_3, 14.00–33.00 wt.% Al_2O_3, 3.34–55.99 wt.% TFeO (total Fe_2O_3 + FeO), 13.68–21.64 wt.% MgO and minor concentrations of NiO (<1.20 wt.%) and TiO_2 (<0.60 wt.%). They have Cr# values [molar $Cr_2O_3/(Cr_2O_3 + Al_2O_3)$] ranging from 18 to 67. Their TFeO and Fe_2O_3 contents (calculated assuming perfect spinel stoichiometry, see Table 6) increase but Cr_2O_3 content decreases with increasing fO_2. Hence, the substitution of Fe^{3+} for Cr and Al in the spinel structure has significant effect on the Cr#, in particular in the high fO_2 cases. The spinel produced in run Cu-6# of the MORB experiments contains 5.62 wt.% Cr_2O_3, 9.53 wt.% Al_2O_3, 67.55 wt.% TFeO, 9.69 wt.% MgO, 0.12 wt.% NiO and 1.02 wt.% TiO_2 (Table 6), showing much higher TFeO and Fe_2O_3 but lower Cr_2O_3, Al_2O_3 and MgO compared to those produced in the Komatiite experiments.

Compositions of garnet and plagioclase are reported in Table 7. Garnet was present only in two MORB runs (MORB-L5 and MORB-L6) at 3.5 GPa and 1200 °C (Table 2). Garnet compositions are pyrope-rich with Mg# = 57–62 and grt/melt K_D^{Fe-Mg} = 0.37–0.52 (Table 6). Run Cu-41# in the MORB experiments contains plagioclase and its composition appears to be Ca-rich.

3.5. Approach to equilibrium

Assessment of major element equilibrium can be made from observations of phase homogeneity and by

considering exchange equilibria between solids and melts. As pointed out in Section 3.4, the Fe–Mg exchange in several runs at relatively reduced conditions did not reach equilibrium due to the significant Fe losses during the experiments, which thus results in somewhat higher ol/, opx/ and cpx/melt Fe–Mg K_D values and higher Mg# values than expected. However, all the major elements at oxidized conditions and all the major elements except Fe and Mg at reduced conditions appear to have approached to equilibrium. This is evidenced by (1) homogeneous compositions (Table 3–7) in each phase within a single run, and (2) the same phase assemblage and very similar phase compositions in the runs with similar experimental conditions (P–T–fO_2) but different durations. For example, MORB-L2 vs. MORB-L3 and Cu-31# vs. Cu-55# (experimental conditions in Table 2) respectively produced the same phase assemblage and nearly same phase compositions (Tables 3–7). Although the Fe–Mg exchange disequilibria in the Fe-loss runs, Cu partitioning for olivine/melt and opx/melt only depends on fO_2 but not related to their Mg# (see Section 3.6). This suggests that Fe–Mg exchange disequilibrium does not significantly affect the Cu partitioning.

Several lines of evidence suggest that Cu partitioning has approached equilibrium. (1) We used $Pt_{95}Cu_{05}$ alloy capsules to provide Cu sources for the experimental charges. Cu diffusion from alloy capsules into silicate melts would avoid continuous Cu loss from the charges during the experiments as in the case of using Cu-free capsules. The Cu activity of a $Pt_{95}Cu_{05}$ alloy capsule was nearly unchanged and the Cu concentration of each phase in the charge at a given P–T–fO_2 condition was buffered by the capsule alloy at a constant value. (2) The H_2O added to experimental charges helps to promote diffusion equilibrium during the experiments. Cu concentrations in all the minerals and melts are homogeneous, indicating that Cu diffusion was rapid and Cu dissolution reached equilibrium. (3) The reproducibility of D_{Cu} at similar experimental conditions (P–T–fO_2) but different durations demonstrates that equilibration was achieved. Again for example Cu-31# vs. Cu-55# and MORB-L2 vs. MORB-L3 (see Table 2 for experimental conditions and Table 8 for D_{Cu} values), $D_{Cu}^{ol/melt} = 0.097 \pm 0.004$ and $D_{Cu}^{spl/melt} = 0.186 \pm 0.048$ for Cu-31# and $D_{Cu}^{ol/melt} = 0.102 \pm 0.005$ and $D_{Cu}^{spl/melt} = 0.189 \pm 0.024$ for Cu-55# are identical within errors, whereas $D_{Cu}^{cpx/melt} = 0.110 \pm 0.023$ for MORB-L2 and $D_{Cu}^{cpx/melt} = 0.134 \pm 0.014$ for MORB-L3 are also identical within errors. (4) The systematic variation of D_{Cu} for ol/, opx/ and spl/melt with fO_2 also indicates Cu partitioning equilibration (see below).

3.6. Copper partitioning

Cu partition coefficients were calculated from the concentrations of Cu in minerals and quenched melts in Tables 3–7. The results are presented in Table 8.

3.6.1. Olivine/melt

The concentration of Cu in olivine ranges from 15 to 1426 ppm and also increases, as in the melts described in Section 3.3, with increasing fO_2. For example, at 1.0 GPa and 1300 °C, it increases from 15 to 30, 46 and 1426 ppm (Table 4) when the estimated fO_2 value increases from FMQ − 1.8 to FMQ + 0.8, +1.2 and +3.8 (Table 2).

Table 8
Mineral/melt Cu partition coefficients.

Run No.	$D^{ol/melt}$	S.D.	$D^{opx/melt}$	S.D.	$D^{cpx/melt}$	S.D.	$D^{grt/melt}$	S.D.	$D^{spl/melt}$	S.D.	$D^{pl/melt}$	S.D.
Cu-50#	0.055	0.003	0.036	0.005					<0.28[†]			
Cu-46#	0.107	0.018							0.232	0.044		
Cu-31#	0.097	0.004							0.186	0.048		
Cu-5#	0.074	0.025							0.248	0.057		
Cu-30#	0.108	0.015							0.217	0.047		
Cu-55#	0.102	0.005							0.189	0.024		
Komatiite-L4	0.053	0.007	0.039	0.007	0.060	0.008			<0.25[†]			
Komatiite-L2	0.038	0.009							<0.30[†]			
Komatiite-L1	0.143	0.019	0.094	0.012	0.066	0.012			0.401	0.081		
Cu-41#					0.038	0.006					0.023	0.009
Cu-6#					0.105	0.054			0.765	0.060		
MORB-L2					0.110	0.023						
MORB-L1					0.093	0.009						
MORB-L3					0.134	0.014						
MORB-L5					0.232	0.044	0.046	0.007				
MORB-L6					0.148	0.009	0.038	0.004				
Cu-35#					0.039	0.018						
Cu-47#					0.017	0.002						
Cu-52#					0.035	0.004						
Cu-43#					0.039	0.002						
Cu-48#					0.018	0.002						

Note: Mineral abbreviations as in Table 2; S.D. = $(Cm\hat{}2(S.D.)gl^2/Cgl^4 + (S.D.)m^2/Cgl^2)^{0.5}$.
[†] Estimated by the imprecise EMP analyses of CuO (<0.04%) in the spl.

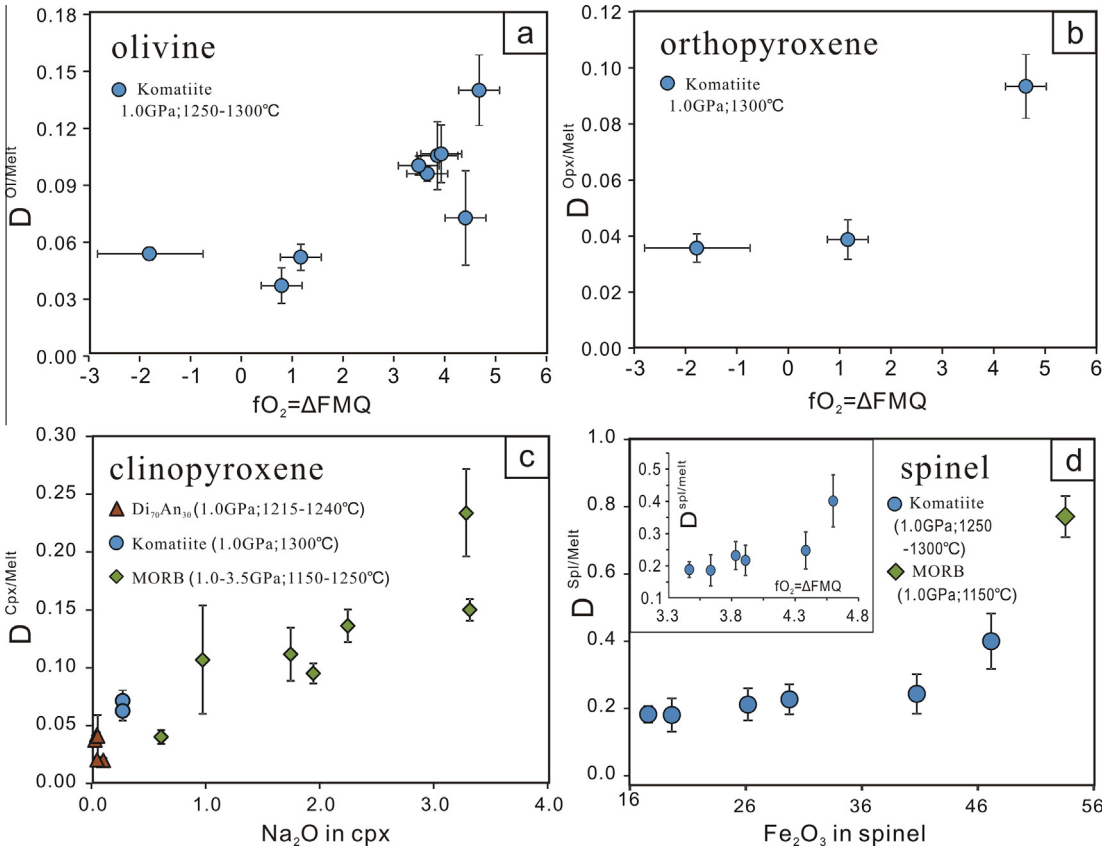

Fig. 6. Cu partition coefficient as a function of fO_2 or mineral composition. (a) $D_{Cu}^{ol/melt}$ vs. fO_2, (b) $D_{Cu}^{opx/melt}$ vs. fO_2, (c) $D_{Cu}^{cpx/melt}$ vs. Na_2O in cpx and (d) $D_{Cu}^{spl/melt}$ vs. Fe_2O_3 in spinel and $D_{Cu}^{spl/melt}$ vs. fO_2 (insert). Error bars are 1σ standard deviation. See Section 3.6 in the text for the details.

The $D_{Cu}^{ol/melt}$ values obtained from all the nine olivine-containing runs range from 0.038 ± 0.009 to 0.143 ± 0.019 (Table 8). An effect of fO_2 on $D_{Cu}^{ol/melt}$ is observed (Fig. 6a). At $fO_2 \leqslant FMQ + 1.2$, $D_{Cu}^{ol/melt}$ values are 0.04–0.06, nearly constant and with the average of 0.05, whereas at $fO_2 > FMQ + 3.0$, they are 0.07–0.14 with the average of 0.12. These indicate that at $fO_2 > FMQ + 1.2$, $D_{Cu}^{ol/melt}$ increases with increasing fO_2. The higher $D_{Cu}^{ol/melt}$ values at the high fO_2 conditions should imply that Cu^{2+} in addition to Cu^{+} is present because Cu^{2+} must more easily substitute Mg^{2+} and Fe^{2+} in the octahedral sites of olivine structure. The possible presence of Cu^{2+} at the high fO_2 conditions is consistent with the results predicted with the data of Cu solubility in melts (see Section 3.3). There is no evidence that $D_{Cu}^{ol/melt}$ varies with Mg# or compositions of olivine. For example (see Tables 2, 4 and 8), the olivines in Cu-46# and Cu-55# have different Mg# (93 vs. 96) but nearly same $D_{Cu}^{ol/melt}$ (0.107 vs. 0.102) due to the similar fO_2 (FMQ + 3.5 vs. FMQ + 3.8), whereas the olivines in Cu-31# and Komatiite-L4 have the same Mg# (94.8) but significantly different $D_{Cu}^{ol/melt}$ (0.097 vs. 0.053) due to the very different fO_2 (FMQ + 3.6 vs. FMQ + 1.2). These demonstrate that $D_{Cu}^{ol/melt}$ is significantly related to fO_2 but not related to the Mg# of olivine. The insensitivity of D_{Cu} on Mg# suggests that Fe losses and ol/melt Fe–Mg exchange disequilibria at reduced conditions also should not significantly affect the $D_{Cu}^{ol/melt}$.

Compared to the previous data, the $D_{Cu}^{ol/melt}$ values of this study (0.04–0.14) are comparable to those (0.02–0.071) obtained by Audetat and Pettke (2006) and those (0.03–0.15) obtained by Lee et al. (2012) with in situ LA-ICP-MS analysis of natural samples. They also have significant overlaps with those (0.08–0.19) obtained by Gaetani and Grove (1997) and those (0.06–0.21) obtained by Fellows and Canil (2012) in laboratory experiments. However, they are over one order of magnitude lower than those (1.2–4.1) experimentally obtained by Adam and Green (2006). The reason for the big differences may be that Adam and Green (2006) conducted experiments with Cu-free noble metal capsules, which could, as pointed out in the introduction, have led to Cu partitioning disequilibrium in their experiments.

3.6.2. Opx/melt

The Cu concentrations in opxs from the three Komatiite runs (Cu-50#, Komatiite-L4 and Komatiite-L1) are 10 ± 1, 34 ± 6 and 484 ± 2 ppm (Table 5) and are 281 ± 8.4, 866 ± 41 and 5125 ± 655 ppm in the corresponding melts (Table 3), producing $D_{Cu}^{opx/melt} = 0.036 \pm 0.005$, 0.039 ± 0.007 and 0.094 ± 0.012 (Table 8), respectively. $D_{Cu}^{opx/melt}$ is also not related to the Mg# of opxs but related to the experimental fO_2. Like $D_{Cu}^{ol/melt}$, $D_{Cu}^{opx/melt}$ also increases

with fO_2 (Fig. 6b) when fO_2 is higher than FMQ + 1.2, again suggesting possible presence of Cu^{2+} at the high fO_2 conditions. However, the nearly constant $D_{Cu}^{ol/melt}$ (0.05) and $D_{Cu}^{opx/melt}$ (0.04) at $fO_2 \leqslant FMQ + 1.2$ (Fig. 6a and b) imply that Cu^{+} was dominant at the relatively low fO_2 conditions.

Compared to previous data, our $D_{Cu}^{opx/melt}$ values are much lower than those (Table S1 and Fig. 1) experimentally obtained using Cu-free noble metal capsules by Adam and Green (2006), Klemme et al. (2006) and Fellows and Canil (2012), but the $D_{Cu}^{opx/melt}$ values at $fO_2 \leqslant FMQ + 1.2$ (0.036 and 0.039) are comparable to $D_{Cu}^{opx/melt} = 0.034$ obtained by Lee et al. (2012) with in situ LA-ICP-MS analysis of natural samples.

3.6.3. Cpx/melt

Like olivine and opx, all the cpxs except the one from run Cu-35# (4.1 ppm Cu) have Cu concentrations higher than 10 ppm (Table 5). Fourteen experiments give the $D_{Cu}^{cpx/melt}$ range from 0.017 ± 0.002 to 0.232 ± 0.044 (Table 8). Pronounced effect on the Cu partitioning appears to be the composition of cpx. As shown in Fig. 6c, $D_{Cu}^{cpx/melt}$ obviously increases with increasing Na_2O in cpx. This implies a possible substitution of Cu^{+} for Na^{+} in addition to the substitution of Cu^{2+} for Mg^{2+} and Fe^{2+} in the cpx structure. Significant effect of fO_2 on $D_{Cu}^{cpx/melt}$ cannot be observed due to the mask of the strong effect of Na_2O, but $D_{Cu}^{cpx/melt} = 0.06$ for run Komatiite-L4 at $fO_2 = FMQ + 1.2$ and $D_{Cu}^{cpx/melt} = 0.07$ for run Komatiite-L1 at $fO_2 = FMQ + 4.6$ suggest that $D_{Cu}^{cpx/melt}$ at the high fO_2 is likely a bit higher than at the low fO_2. Bulk composition or melt composition appears to have no effect on the $D_{Cu}^{cpx/melt}$. As shown in Fig. 6c, all the cpxs crystallizing from the Komatiite, MORB and Di-An compositions actually have identical $D_{Cu}^{cpx/melt}$ within errors when the Na_2O content in cpx is less than 1.0%. This indicates that at least for the mafic compositions investigated, variation in melt composition does not significantly affect the cpx/melt Cu partitioning.

Compared to previous data, our $D_{Cu}^{cpx/melt}$ are also obviously lower than those (>0.35) obtained experimentally by Hart and Dunn (1993) and by Adam and Green (2006), but are comparable to those obtained by Paster et al. (1974), Halter et al. (2004), Audetat and Pettke (2006) and Lee et al. (2012) with natural samples (see Table S1).

3.6.4. Spinel/melt

Among the nine Komatiite runs, six runs with fO_2 higher than FMQ + 3 produced spinel containing 0.16–0.38 wt.% CuO (Table 6), which exceed the 0.04 wt.% detection limit of EMP. The calculated $D_{Cu}^{spl/melt}$ values for these runs range from 0.19 ± 0.05 to 0.40 ± 0.08 (Table 8) with the average of 0.25 ± 0.05. These $D_{Cu}^{spl/melt}$ values are comparable to 0.22 obtained by Lee et al. (2012) with natural samples, but 10 times lower than the only published value of 3.1 experimentally obtained by Klemme et al. (2006) (Table S1). For other three runs (Cu-50#, Komatiite-L2 and Komatiite-L4) at relatively reduced ($\leqslant$FMQ + 1.2) conditions, no precise $D_{Cu}^{spl/melt}$ values can be obtained since the EMP CuO contents (0.01, 0.03 and 0.03 wt.%, respectively) in the spinels from the three runs (Table 6) are lower than the EMP detection limit. The $D_{Cu}^{spl/melt}$ values for the three runs should be <0.28, <0.25 and <0.30, respectively, if $D_{Cu}^{spl/melt}$ is calculated using these imprecise EMP CuO analyses. The "<" (means "lower") is because the EMP method overestimates Cu concentration when Cu is lower than ~400 ppm (see Section 2.6). These roughly estimated values thus indicate that the $D_{Cu}^{spl/melt}$ at relatively reduced conditions should not be higher than those at the oxidized conditions.

The six good $D_{Cu}^{spl/melt}$ values from the Komatiite experiments vs. Fe_2O_3 in spinel and fO_2 were plotted in Fig. 6d and the insert. From these figures, we can clearly see the effects of these two parameters on the partitioning: $D_{Cu}^{spl/melt}$ increases with increasing fO_2 and spinel Fe_2O_3, i.e., $D_{Cu}^{spl/melt}$ decreases with decreasing fO_2 and spinel Fe_2O_3. As seen in the insert of Fig. 6d, if the trend with fO_2 variation is extended from $fO_2 = FMQ + 3.5$ to $fO_2 = FMQ + 1.2$ and lower, then the $D_{Cu}^{spl/melt}$ values at $fO_2 \leqslant FMQ + 1.2$ would be lower than 0.19. Furthermore, the effects of fO_2 and spinel Fe_2O_3 on the partitioning again suggest that both Cu^{2+} and Cu^{+} were possibly coexisting in the melts at high fO_2 and that there were possible substitutions of Cu^{2+} for $Fe^{2+} + Mg^{2+}$ and of $Cu^{+} + Fe^{3+}$ for $2(Fe^{2+} + Mg^{2+})$ in the spinel structure. The spinel produced in run Cu-6# of the MORB experiments has $D_{Cu}^{spl/melt} = 0.77 \pm 0.06$, which is the highest among all the $D_{Cu}^{spl/melt}$ values. This is due to its very high TFeO and Fe_2O_3 (Table 6), again indicating significant effect of TFeO or Fe_2O_3 in spinel on the Cu partitioning.

3.6.5. Garnet/melt and plagioclase/melt

In the two garnet-containing runs (MORB-L5 and MORB-L6), the Cu concentrations are 164 ± 21 and 146 ± 12 ppm in the garnets (Table 7) and are 3574 ± 320 and 3817 ± 242 ppm in the corresponding melts (Table 3), producing $D_{Cu}^{grt/melt} = 0.038 \pm 0.004$ and 0.046 ± 0.007 (Table 8). These two values are one order of magnitude lower than those (0.41–0.69) determined experimentally by Yurimoto and Ohtani (1992) and Adam and Green (2006). The very low $D_{Cu}^{grt/melt}$ obtained in this study indicate that Cu is most incompatible among silicate minerals, in agreement with the results of Lee et al. (2012) (Table S1). We also calculated the Cu partition coefficient between plagioclase and melt in run Cu-41#, the result is Dpl/melt Cu = 0.023 ± 0.009 (Table 8).

In summary, $D_{Cu}^{mineral/melt}$ for ol, opx, spl and possibly cpx increase with increasing fO_2 when $fO_2 > FMQ + 1.2$, while $D_{Cu}^{mineral/melt}$ for cpx and spl also increase with increasing Na_2O in cpx and Fe_2O_3 in spl, respectively. In the investigated P–T–fO_2 conditions, the D_{Cu} values are 0.04–0.14 for ol, 0.04–0.09 for opx, 0.02–0.23 for cpx, 0.19–0.77 for spl and 0.03–0.05 for grt. These results confirm that Cu in all the non-sulfide minerals of the upper mantle is highly incompatible ($D_{Cu} < \sim 0.2$) except for the high-Fe spinel, in which Cu is moderately incompatible ($D_{Cu} = 0.4$–0.8). Therefore, if sulfide is absent during mantle partial melting and magmatic differentiation, Cu must be enriched in the derived melts. For the convenience to applications with the interested workers, we recommend based on the above experimental results that the mean D_{Cu} values at

$fO_2 \leqslant FMQ + 1.2$ (reduced conditions) are $D_{Cu}^{ol/melt} = 0.05$, $D_{Cu}^{opx/melt} = 0.04$, $D_{Cu}^{cpx/melt} = 0.06$, $D_{Cu}^{spl/melt} = 0.19$ and $D_{Cu}^{grt/melt} = 0.03$, whereas at $fO_2 > FMQ + 3$ (oxidized conditions) are $D_{Cu}^{ol/melt} = 0.12$, $D_{Cu}^{opx/melt} = 0.09$, $D_{Cu}^{cpx/melt} = 0.13$, $D_{Cu}^{spl/melt} = 0.25$ and $D_{Cu}^{grt/melt} = 0.05$.

4. APPLICATIONS: CU BEHAVIOR DURING MANTLE MELTING

All the olivine, opx and spinel produced at this study from the Komatiite experiments and the compositions for these minerals and their corresponding melts overlap the compositions of phases produced in the peridotite melting (e.g., Walter, 1998). Although the cpxs were produced from three different bulk compositions (Komatiite, MORB and Di–An), the results (see Section 3.6.3) show that bulk composition has no effect on the $D_{Cu}^{cpx/melt}$. Importantly, the experimental $D_{Cu}^{mineral/melt}$ values for ol, opx, cpx, spl and grt from this study are comparable to those obtained by Audetat and Pettke (2006) and Lee et al. (2012) with in situ LA-ICP-MS analysis of natural samples. Hence, our experimental results on Cu partitioning are applicable to the mantle melting.

The main magmas derived from the upper mantle include MORBs, arc basalts and OIBs, which generally have Cu contents in the range of 60–80, 50–100 and 80–120 ppm, respectively (Fellows and Canil, 2012; Lee et al., 2012). It has been widely accepted that MORBs form generally by 6–15% melting of mantle peridotites (Langmuir et al., 1992; Kinzler and Grove, 1992; Bezos and Humler, 2005; Workman and Hart, 2005; Niu and O'Hara, 2008; Putirka et al., 2011), whereas arc basalts are produced by 10–25% melting of the mantle wedge peridotites metasomatized by slab-derived fluids and/or melts (e.g., Tatsumi et al., 1983; Plank and Langmuir, 1988; Pearce and Parkinson, 1993). The genesis of OIBs is complicated. They may form by <5% melting of CO_2-bearing peridotites (Mckenzie and O'Nions, 1995; Hirose, 1997; Dasgupta et al., 2007), or by higher degree melting of mineralogically heterogeneous mantle regions such as the pyroxenite/eclogite-containing peridotite regions (Hauri, 1996; Hirschmann et al., 2003; Kogiso et al., 2003, 2004; Ren et al., 2004; Sobolev et al., 2005, 2007; Herzberg, 2006, 2011; Le Roux et al., 2010, 2011) and the metasomatized peridotite regions with hornblende dikes (Pilet et al., 2004, 2005 and Pilet et al., 2008). They may also form by MORB-eclogite partial melt and fertile peridotite reaction at the subsolidus of mantle peridotite (Mallik and Dasgupta, 2012). It is difficult to clearly figure out the factors controlling the Cu contents of OIBs due to the complexity of their source composition and mineralogy, formation ways and melting degree. In the following sections, we drop OIBs, but only focus on discussion of the controls of Cu behavior during the generations of MORBs and arc basalts using our new Cu partition coefficients. Our goal here is to assess whether the Cu contents of MORBs and arc basalts can be explained by sulfide-free mantle sources in light of the new partition coefficients and then to infer the general fO_2 in their source mantles based on the presence or absence of sulfide. Our experiments show that the $D_{Cu}^{mineral/melt}$ values for ol, opx, cpx and spl vary with change of fO_2. Hence, Cu behaviors during the mantle melting at low ($\leqslant FMQ + 1.2$) and high ($> FMQ + 3$) fO_2 conditions were calculated and discussed, respectively.

4.1. The control of Cu behavior at reduced conditions

We here consider the hypothetical case in which mantle melting is sulfide-absent so that the behavior of Cu is controlled only by the silicate minerals. It is in general accepted that for the genesis of mantle-derived magmas, neither pure fractional melting nor pure batch melting is realistic, but a near-fractional melting and an accumulated fractional melting are widely adopted (e.g., Langmuir et al., 1992; Niu, 1997; Kushiro, 2001; Lee et al., 2012). The application of a near-fractional or an accumulated fractional model does not result in importantly different results. We here use a near-fractional melting model as described by Lee et al. (2012) to calculate the Cu contents of aggregate melts as a function of source initial Cu abundance, bulk D_{Cu} and melting degree. In this melting model, the instantaneous fractional melts coexisting with peridotite residues are generated by fractional melting and then pooled. We assume a mantle residue after melt extraction consisting of 60 wt.% ol, 20 wt.% opx, 18 wt.% cpx and 2 wt.% spl (or grt), and then select $D_{Cu}^{mineral/melt}$ values to calculated the bulk D_{Cu}. Based on the mean D_{Cu} values obtained in this study at $fO_2 \leqslant FMQ + 1.2$, $D_{Cu}^{ol/melt} = 0.05$, $D_{Cu}^{opx/melt} = 0.04$, $D_{Cu}^{cpx/melt} = 0.06$ and $D_{Cu}^{spl/melt} = 0.19$ were selected for the calculations at reduced conditions. Both spinel and garnet are minor amounts of phases during mantle melting and thus garnet ($D_{Cu}^{grt/melt} = 0.04$) instead of spinel in the residue does not result in a substantial change of the bulk D_{Cu}. Using these D_{Cu} values and mineral modes, bulk $D_{Cu} = 0.053$ was obtained at the reduced conditions. With this bulk D_{Cu}, the variations of calculated Cu contents in the partial melts with source initial Cu

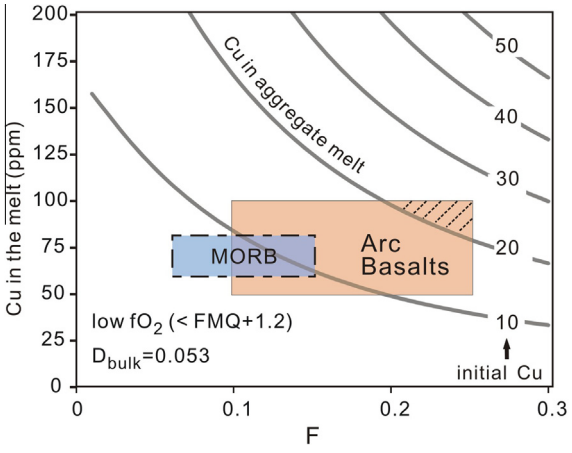

Fig. 7. Variation of Cu concentration in the aggregate melt with mantle initial Cu abundance (from 10 to 50 ppm) and melting degree (F) for the near-fractional melting of a sulfide-free peridotite with bulk $D_{Cu} = 0.053$ at reduced ($fO_2 < FMQ + 1.2$) conditions. For the details on the near-fractional melting calculations and the fields of MORB and arc basalts, see Section 4.1.

abundance and melting degree were shown in Fig. 7. For comparison, the ranges of Cu contents and melting degrees for MORBs and arc basalts were also plotted in this figure.

As shown in Fig. 7, with bulk $D_{Cu} = 0.053$ and 6–15% melting degree (e.g., Kinzler and Grove, 1992; Bezos and Humler, 2005; Workman and Hart, 2005), the 60–80 ppm Cu contents in MORBs (Fellows and Canil, 2012; Lee et al., 2012) only can be explained with <~14 ppm Cu in the source mantle. Cu abundance lower than 14 ppm is too low compared to the accepted Cu abundance of 20–30 ppm in the upper mantle (Sun, 1982; O'Neill, 1991). Therefore, the presence of residual sulfide is necessary during the MORB generation to reconcile the mismatch between the observed Cu contents and the accepted mantle Cu abundance. In other words, only the addition of sulfide to the residue to MORBs can elevate the bulk D_{Cu} and render the observed Cu contents of 60–80 ppm well match the mantle Cu abundance of 20–30 ppm. This inference is consistent with the widespread existence of sulfides in the mantle peridotite xenoliths (e.g., Lorand, 1990; McInnes et al., 2001; Lee, 2002; Alard et al., 2011).

With bulk $D_{Cu} = 0.053$ and 10–25% melting degree (e.g., Plank and Langmuir, 1988; Pearce and Parkinson, 1993), only less than 10% arc basalts with high Cu contents (80–100 ppm) can be explained using 20–25 ppm mantle initial Cu. More than 90% arc basalts still require the addition of sulfide to the residues to elevate the bulk D_{Cu} in order that their observed Cu contents of 50–100 ppm (Fellows and Canil, 2012; Lee et al., 2012) well match the accepted mantle Cu abundance of 20–30 ppm. This suggests that sulfide presence would also generally be required if arc basalts were produced at reduced conditions. It can be inferred further from Fig. 7 that sulfide during the genesis of arc basalts must be necessary if the Cu abundance in the arc mantle is in excess of 20–30 ppm. Many studies (e.g., Noll et al., 1996; De Hoog et al., 2001; Wallace, 2001; Rowe et al., 2009; Wallace and Edmonds, 2011) demonstrated that arc basalts relative to MORBs are more hydrous and enriched in Cl, S and chalcophile elements in addition to incompatible elements. The enrichment of S, Cu and other chalcophile elements is attributed to metasomatism of the mantle wedge by slab-derived fluids and/or melts (Noll et al., 1996; De Hoog et al., 2001; McInnes et al., 2001; Sun et al., 2003, 2004a, 2004b; Mungall et al., 2006; Wallace and Edmonds, 2011). One set of experiments this year (Jégo and Dasgupta, 2013) have demonstrated that reduced, H_2S-rich fluid can be a sufficient agent of addition of S from slab to mantle wedge.

Assuming the mantle Cu abundance not lower than 20 ppm, the Cu contents of MORBs and >90% arc basalts cannot be explained by sulfide-absent melting in light of our partition coefficients at reduced conditions. Hence sulfide-present melting is required for the genesis of MORB and the overwhelming majority of arc basalts if only reduced conditions are considered. This result is consistent with that of Lee et al. (2012) since their bulk D_{Cu} (0.045) for silicate minerals is very close to 0.053 used here. However, this result is different from that of Fellows and Canil (2012), whose calculations suggested that the Cu contents in

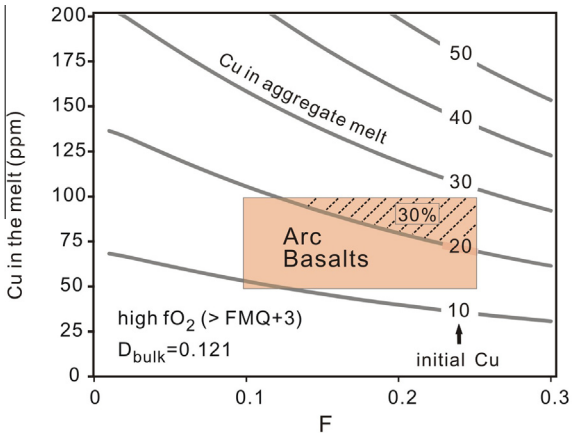

Fig. 8. Variation of Cu concentration in the aggregate melt with mantle initial Cu abundance (from 10 to 50 ppm) and melting degree (F) for the near-fractional melting of a sulfide-free peridotite with bulk $D_{Cu} = 0.121$ at oxidized ($fO_2 > FMQ + 3$) conditions. The obliquely lined field indicates that ~30% arc basalts (with 70–100 ppm Cu) could be generated at the high fO_2 conditions, assuming 20–30 ppm Cu in the source mantle.

MORBs and arc basalts can be explained by considering only the silicate behavior. The difference is mainly due to the fact that our bulk $D_{Cu} = 0.053$ used here is notably lower than those (0.11–0.13) used by Fellows and Canil (2012). Hence, applications of different D_{Cu} values may result in fundamentally different interpretation of the mantle source mineralogy (i.e., sulfide-present or sulfide-absent).

4.2. The control of Cu behavior at oxidized conditions

At fO_2 higher than FMQ + 2 that destabilize sulfides (Carroll and Rutherford, 1987; Jugo et al., 2005, 2010), sulfides during mantle melting are absent. The behavior of Cu at oxidized conditions will thus be controlled only by silicate minerals. Based on the mean D_{Cu} values obtained in this study at $fO_2 > FMQ + 3$, $D_{Cu}^{ol/melt} = 0.12$, $D_{Cu}^{opx/melt} = 0.09$, $D_{Cu}^{cpx/melt} = 0.13$ and $D_{Cu}^{spl/melt} = 0.25$ were selected for the calculation of the bulk D_{Cu} at oxidized conditions. With these D_{Cu} values and assuming a mantle residue consisting of the same mineral modes as in reduced conditions, the bulk D_{Cu} is 0.121. We here still use the near-fractional melting model to calculate the Cu contents of the pooled/aggregate melts. With the bulk $D_{Cu} = 0.121$, the variations of calculated Cu contents in the partial melts with source initial Cu abundance and melting degree were shown in Fig. 8.

The bulk $D_{Cu} = 0.121$ at oxidized conditions cannot be applied to MORB genesis, since MORB mantle is reduced with fO_2 lower than FMQ + 0.5 (e.g., Bezos and Humler, 2005; Kelley and Cottrell, 2009; Cottrell and Kelley, 2011). In Fig. 8, we only plot the ranges of Cu contents and melting degrees of arc basalts to see whether their Cu contents can be explained with the bulk D_{Cu} obtained at oxidized conditions. It can been seen from Fig. 8 that ~30% arc basalts with 70–100 ppm Cu (the obliquely lined field) can be explained with the bulk

$D_{Cu} = 0.121$, assuming 20–30 ppm Cu in the source mantle. In other words, it is possible for these high Cu arc basalts to be produced at oxidized, sulfide-absent conditions. Other arc basalts (70%) cannot be explained and thus do not form by sulfide-absent melting at oxidized conditions unless the mantle Cu abundance is lower than 20 ppm.

This result that high Cu (>70 ppm) arc basalts may be produced by oxidized, sulfide-absent melting is different from that of Lee et al. (2012), who suggested that arc basalts similar to MORBs were produced by reduced, sulfide-present melting. The reason for this difference is that Lee et al. (2012) assumed Cu partition coefficients for silicate minerals not varying with fO_2 and thus only used a constant bulk $D_{Cu}^{silicate/melt} = 0.045$, which is much lower than our silicate bulk $D_{Cu} = 0.121$ at oxidized conditions. Again, applications of different D_{Cu} values may result in fundamentally different interpretation of the mantle source mineralogy.

4.3. Is the fO_2 of arc mantle highly heterogeneous?

Observations have shown that most arc magmas are more (up to 3 logfO_2 units) oxidized than MORBs (e.g., Carmichael, 1991; De Hoog et al., 2001; Kelley and Cottrell, 2009). There is, however, no consensus on whether primitive arc basalts and their source mantle are more oxidized than MORBs. Some studies (McInnes et al., 2001; Mungall, 2002; Kelley and Cottrell, 2009 and Prouteau and Scaillet, 2013) suggested that the high fO_2 of arc lavas is directly inherited from an oxidized mantle source because mantle wedge will likely be oxidized through addition of slab-derived fluids or melts rich in oxidized components, such as Fe^{3+} and S^{6+} species (sulfate). Although this view is plausible, direct evidence recording high fO_2 arc mantle remains rare. Indeed, some peridotite xenoliths from arc environments, such as those from Simcoe near the Washington Cascades, Japan, and the Solomon Islands (Brandon and Draper, 1996; Parkinson and Arculus, 1999), record mineral barometry fO_2 up to FMQ + 2, and the amphibole-bearing mini-xenoliths from western Mexico record fO_2 up to FMQ + 4 (Blatter and Carmichael, 1998). However, the majority of continental peridotite xenoliths, some of which may have originated in arc settings, have fO_2 ranging from FMQ − 2 to FMQ + 1 (Mattioli and Wood, 1986; Wood and Virgo, 1989; Ballhaus et al., 1991), overlapping the fO_2 of MORBs, and lower than that of most arc magmas. On the other hand, Lee et al. (2005, 2010, 2012), based on the similarities of V/Sc, Zn/Fe, and Cu systematics of primitive arc basalts and MORBs, demonstrated that mantle wedge is not more oxidized than the MORB mantle. They thus concluded that the high fO_2 of arc magmas must be in part a consequence of shallow-level differentiation processes. They also argued that barometric fO_2 of mantle xenoliths is not necessarily representative of the fO_2 of the asthenospheric mantle of arc magma sources, because nearly all peridotite xenoliths so far originated from the lithospheric mantle that have likely undergone oxidizing metasomatic processes. Hence, whether arc magmas can form at oxidized conditions and whether the fO_2 of mantle wedge is heterogeneous remain debated.

The presence or absence of sulfide during mantle melting is of key importance in understanding the general fO_2 of the mantle source since the stability of sulfide is a function of fO_2. The valence state and speciation of S in silicate melts are redox-sensitive. The fO_2 for the transition from sulfide-leading S (S^{2-}) to sulfate-leading S (S^{6+}) is around FMQ + 1. At $fO_2 <$ FMQ + 0.5, the dominant oxidation state is S^{2-}, which stabilizes sulfides, whereas at $fO_2 >$ FMQ + 1.5 sulfate is the dominant S species (Carroll and Rutherford, 1987; Jugo et al., 2005, 2010). We have calculated and discussed the possibilities of sulfide presence and absence during the genesis of arc basalts based on our new Cu partition coefficients. The relevant results may provide some constraints on the general fO_2 of the arc mantle. As discussed above, assuming 20–30 ppm Cu in the mantle source, the Cu contents of more than 90% arc basalts cannot be explained with the silicate bulk $D_{Cu} = 0.053$ at reduced conditions (Fig. 7) and thus require sulfide-present melting. The Cu contents of 70% arc basalts also cannot be explained with the silicate bulk $D_{Cu} = 0.121$ at oxidized conditions (Fig. 8). This excludes that these arc basalts form at oxidized conditions, but conversely implies that at least 70% arc basalts form only by reduced, sulfide-present melting. Combining the two calculated results together, we conclude that most arc basalts must form by sulfide-present melting and the relevant arc mantle must have fO_2 lower than FMQ + 1.5, even lower than FMQ + 0.5 that overlaps the fO_2 of the MORB mantle. This conclusion is to a large extent consistent with the argument of Lee et al. (2005, 2010) and Lee et al. (2012). However, ~30% arc basalts with high Cu contents (70–100 ppm) can be explained with the silicate bulk D_{Cu} at oxidized conditions (Fig. 8). This suggests that high Cu arc basalts may likely form by the melting of an oxidized, sulfide-absent mantle, and the relevant arc mantle fO_2 could be higher than FMQ + 3 in light of the experimental fO_2. If high fO_2 regions in the arc mantle is indeed present, then it means that the fO_2 of arc magmas source regions are in high heterogeneity. It should be noted that the bulk $D_{Cu} = 0.121$ used here is derived from the average $D_{Cu}^{mineral/melt}$ for ol, opx, cpx and spl at the high end fO_2 (>FMQ + 3) conditions. The result constrained by this bulk D_{Cu} does not mean that so high fO_2 is necessarily present in the arc mantle. However, if we use a bulk D_{Cu} obtained at a moderately high fO_2, such as bulk $D_{Cu} = 0.08$ at FMQ + 2 (estimated from Fig. 6 and Table 8), then there remains at least 15% high Cu arc basalts that may be explained with this bulk D_{Cu}. Therefore, some high Cu arc basalts may form at oxidized (>FMQ + 2), sulfide-absent conditions and there is a possibility that some high fO_2 regions are present in the arc mantle.

Based on the discussions above, we can conclude that the fO_2 of arc mantle may generally be lower than FMQ + 1.5, even cannot be distinguished from those of the MORB as suggested by Lee et al. (2005, 2010, 2012). Alternatively, it is highly heterogeneous with fO2 variation from lower than FMQ + 1.5 in most regions to higher than FMQ + 2, even higher than FMQ + 3 in

some regions. Existing studies suggested that the fO_2 in the upper mantle probably changed with time (Wood, 1991; Frost and McCammon, 2008; Creighton et al., 2009). Some peridotite xenoliths from arc settings record barometric fO_2 up to FMQ + 2 (Brandon and Draper, 1996; Parkinson and Arculus, 1999), even up to FMQ + 4 (Blatter and Carmichael, 1998). The olivine hosted melt inclusions from primitive basaltic lavas in the Cascades also record fO_2 up to FMQ + 2.4 (Rowe et al., 2009). These xenoliths and melt inclusions should to a certain extent, if not fully, indicate the possibility of some high fO_2 regions present in the arc mantle. Anyway, more direct evidence remains required and more explorations and tests should be carried out in the future.

5. CONCLUSIONS

(1) This study used $Pt_{95}Cu_{05}$ alloy capsules to provide the source of Cu to determine $D_{Cu}^{mineral/melt}$ for ol, opx, cpx, spl and grt at the P–T–fO_2 conditions of upper mantle. The experiments with this capsule technique have produced minerals and melts with high Cu concentrations (>10 ppm), which reduces analytical uncertainty with the LA-ICP-MS. The Cu-bearing capsules also have buffered the Cu concentrations in the minerals and melts and thus facilitated the attainment of partitioning equilibrium.

(2) $D_{Cu}^{mineral/melt}$ for ol, opx, spl and possibly cpx increase with increasing fO_2 when $fO_2 >$ FMQ + 1.2, while $D_{Cu}^{mineral/melt}$ for cpx and spl also increase with increasing Na_2O in cpx and Fe_2O_3 in spl, respectively. In the investigated P–T–fO_2 conditions, the D_{Cu} values are 0.04–0.14 for ol, 0.04–0.09 for opx, 0.02–0.23 for cpx, 0.19–0.77 for spl and 0.03–0.05 for grt. These results confirm that Cu in all the non-sulfide minerals of the upper mantle is highly incompatible ($D_{Cu} <$ ~0.2) except for the high-Fe spinel, in which Cu is moderately incompatible ($D_{Cu} = 0.4$–0.8). Therefore, if sulfide is absent during mantle partial melting and magmatic differentiation, Cu must be enriched in the derived melts.

(3) The following results can be inferred from the model calculations with the mean $D_{Cu}^{mineral/melt}$ values obtained at $fO_2 \leqslant$ FMQ + 1.2 and >FMQ + 2: (a) MORBs and most arc basalts must form by reduced, sulfide-present partial melting unless the upper mantle Cu abundance is lower than 20 ppm. This constrains the fO_2 in most arc mantle regions lower than FMQ + 1.5 based on sulfide attending the melting. (b) High Cu (>70 ppm) arc basalts may form by oxidized, sulfide-absent partial melting and the relevant arc mantle fO_2 could be higher than FMQ + 2. Therefore, there is a possibility that the fO_2 of arc mantle are highly heterogeneous, varying from <FMQ + 1.5 in most regions to >FMQ + 2 in some regions. We suggest that the high fO_2 possibility in the arc mantle should be explored and tested further in the future.

ACKNOWLEDGEMENTS

We would like to thank H. Schulze for the preparation of polished sections, D. Krausse and L.L. Chen for help with the electron microprobe analyses, X.L. Tu for help with the LA-ICP-MS analyses at Guangzhou and H. Keppler, C. McCammon and H. Ni for help during the experiments when the first and second authors were in Bayreuth. The authors gratefully acknowledge the financial supports from the NBRP of China (2014CB440802), the NSF of China (41373061, 40825010, 41121002, 41173070, 41090373) and 135 project of GIGCAS (Y234152001) to X.L. Xiong and M.S. Song and from the Bayerisches Geoinstitut to H. Keppler. We also like to thank Dr. H. Ni for comments on the early version of the manuscript. Reviews by Cin-Ty Lee and Zoltan Zajacz and the comments of Rajdeep Dasgupta (associate editor) have greatly helped to improve the paper. This is contribution No.1753 from GIGCAS.

APPENDIX A. SUPPLEMENTARY DATA

Supplementary data associated with this article can be found, in the online version, at http://dx.doi.org/10.1016/j.gca.2013.09.039.

REFERENCES

Adam J. and Green T. (2006) Trace element partitioning between mica-and amphibole-bearing garnet lherzolite and hydrous basanitic melt: 1. Experimental results and the investigation of controls on partitioning behaviour. *Contrib. Mineral. Petrol.* **152**, 1–17.

Alard O., Lorand J. P., Reisberg L., Bodinier J. L., Dautria J. M. and O'Reilly S. Y. (2011) Volatile-rich metasomatism in montferrier xenoliths (Southern France): Implications for the abundances of chalcophile and highly siderophile elements in the subcontinental mantle. *J. Petrol.* **52**, 2009–2045.

Audetat A. and Pettke T. (2006) Evolution of a porphyry-Cu mineralized magma system at Santa Rita, New Mexico (USA). *J. Petrol.* **47**, 2021–2046.

Ballhaus C., Berry R. F. and Green D. H. (1990) Oxygen fugacity controls in the earths upper mantle. *Nature* **348**, 437–440.

Ballhaus C., Berry R. F. and Green D. H. (1991) High pressure experimental calibration of the olivine-orthopyroxene-spinel oxygen geobarometer: implications for the oxidation state of the upper mantle. *Contrib. Mineral. Petrol.* **107**, 27–40.

Bezos A. and Humler E. (2005) The Fe3+/ΣFe ratios of MORB glasses and their implications for mantle melting. *Geochim. Cosmochim. Acta* **69**, 711–725.

Blatter D. L. and Carmichael I. S. (1998) Hornblende peridotite xenoliths from central Mexico reveal the highly oxidized nature of subarc upper mantle. *Geology* **26**, 1035–1038.

Bose K. and Ganguly J. (1995) Quartz-coesite transition revisited - reversed experimental-determination at 500–1200°C and retrieved thermochemical properties. *Am. Mineral.* **80**, 231–238.

Bougault H. and Hekinian R. (1974) Rift valley in the Atlantic Ocean near 36°50′N: Petrology and geochemistry of basaltic rocks. *Earth Planet. Sci. Lett.* **24**, 249–261.

Brandon A. D. and Draper D. S. (1996) Constraints on the origin of the oxidation state of mantle overlying subduction zones: an example from Simcoe, Washington, USA. *Geochim. Cosmochim. Acta* **60**, 1739–1749.

Carmichael I. S. E. (1991) The redox states of basic and silicic magmas - a reflection of their source regions. *Contrib. Mineral. Petrol.* **106**, 129–141.

Carroll M. R. and Rutherford M. J. (1987) The stability of igneous anhydrite - experimental results and implications for sulfur behavior in the 1982 El-Chichon trachyandesite and other evolved magmas. *J. Petrol.* **28**, 781–801.

Chou I.-M. (1987) Oxygen buffer and hydrogen sensor techniques at elevated pressures and temperatures. *Hydrothermal experimental techniques*, 61–99.

Cottrell E. and Kelley K. A. (2011) The oxidation state of Fe in MORB glasses and the oxygen fugacity of the upper mantle. *Earth Planet. Sci. Lett.* **305**, 270–282.

Creighton S., Stachel T., Matveev S., Hofer H., McCammon C. and Luth R. W. (2009) Oxidation of the Kaapvaal lithospheric mantle driven by metasomatism. *Contrib. Mineral. Petrol.* **157**, 491–504.

Dasgupta R., Hirschmann M. M. and Smith N. D. (2007) Partial melting experiments of peridotite CO2 at 3 GPa and genesis of alkalic ocean island basalts. *J. Petrol.* **48**, 2093–2124.

De Hoog J., Mason P. and Van Bergen M. (2001) Sulfur and chalcophile elements in subduction zones: constraints from a laser ablation ICP-MS study of melt inclusions from Galunggung Volcano, Indonesia. *Geochim. Cosmochim. Acta* **65**, 3147–3164.

Dostal J., Dupuy C., Carron J., Guen Le., de Kerneizon M. and Maury R. (1983) Partition coefficients of trace elements: application to volcanic rocks of St. Vincent, West Indies. *Geochim. Cosmochim. Acta* **47**, 525–533.

Droop G. (1987) A general equation for estimating Fe3+ concentrations in ferromagnesian silicates and oxides from microprobe analyses, using stoichiometric criteria. *Mineralogical magazine* **51**, 431–435.

Ewart A. and Griffin W. (1994) Application of proton-microprobe data to trace-element partitioning in volcanic rocks. *Chem. Geol.* **117**, 251–284.

Ewart A., Bryan W. and Gill J. (1973) Mineralogy and geochemistry of the younger volcanic islands of Tonga, SW Pacific. *J. Petrol.* **14**, 429–465.

Fellows S. A. and Canil D. (2012) Experimental study of the partitioning of Cu during partial melting of Earth's mantle. *Earth Planet. Sci. Lett.* **337**, 133–143.

Frost B. R. (1991) Introduction to oxygen fugacity and its petrologic importance. *Rev. Mineral. Geochem.* **25**, 1–9.

Frost D. J. and McCammon C. A. (2008) The redox state of Earth's mantle. *Annu. Rev. Earth Planet. Sci.* **36**, 389–420.

Gaetani G. A. and Grove T. L. (1997) Partitioning of moderately siderophile elements among olivine, silicate melt, and sulfide melt constraints on core formation in the Earth and Mars. *Geochim. Cosmochim. Acta* **61**, 1829–1846.

Haas J., Robie R. and Heinrich C. A. (1973) Thermodynamic data for wüstite, $Fe_{0.947}O$, magnetite, Fe_3O_4, and hematite, Fe_2O_3. *Eos Trans. AGU* **54**, 483.

Halter W. E., Pettke T. and Heinrich C. A. (2004) Laser-ablation ICP-MS analysis of silicate and sulfide melt inclusions in an andesitic complex I: analytical approach and data evaluation. *Contrib. Mineral. Petrol.* **147**, 385–396.

Hart S. R. and Dunn T. (1993) Experimental cpx/melt partitioning of 24 trace elements. *Contrib. Mineral. Petrol.* **113**, 1–8.

Hauri E. H. (1996) Major-element variability in the Hawaiian mantle plume. *Nature* **382**, 415–419.

Herzberg C. (2006) Petrology and thermal structure of the Hawaiian plume from Mauna Kea volcano. *Nature* **444**, 605–609.

Herzberg C. (2011) Identification of source lithology in the Hawaiian and Canary Islands: implications for origins. *J. Petrol.* **52**, 113–146.

Hirose K. (1997) Partial melt compositions of carbonated peridotite at 3 GPa and role of CO2 in alkali-basalt magma generation. *Geophys. Res. Lett.* **24**, 2837–2840.

Hirschmann M. M., Kogiso T., Baker M. B. and Stolper E. M. (2003) Alkalic magmas generated by partial melting of garnet pyroxenite. *Geology* **31**, 481–484.

Hofmann A. W. (1988) Chemical differentiation of the Earth: the relationship between mantle, continental crust, and oceanic crust. *Earth Planet. Sci. Lett.* **90**, 297–314.

Holzheid A. and Lodders K. (2001) Solubility of copper in silicate melts as function of oxygen and sulfur fugacities, temperature, and silicate composition. *Geochim. Cosmochim. Acta* **65**, 1933–1951.

Hsu L. (1967) Melting of fayalite up to 40 kilobars. *J. Geophys. Res.* **72**, 4235–4244.

Jakobsson S. and Oskarsson N. (1994) The system CO in equilibrium with graphite at high pressure and temperature: An experimental study. *Geochim. Cosmochim. Acta* **58**, 9–17.

Jégo S. and Dasgupta R. (2013) Fluid-present melting of sulfide-bearing ocean-crust: experimental constraints on the transport of sulfur from subducting slab to mantle wedge. *Geochim. Cosmochim. Acta* **110**, 106–134.

Jenner F. E., O'Neill H. S. T., Arculus R. J. and Mavrogenes J. A. (2010) The magnetite crisis in the evolution of arc-related magmas and the initial concentration of Au, Ag and Cu. *J. Petrol.* **51**, 2445–2464.

Jugo P. J., Luth R. W. and Richards J. P. (2005) Experimental data on the speciation of sulfur as a function of oxygen fugacity in basaltic melts. *Geochim. Cosmochim. Acta* **69**, 497–503.

Jugo P. J., Wilke M. and Botcharnikov R. E. (2010) Sulfur K-edge XANES analysis of natural and synthetic basaltic glasses: implications for S speciation and S content as function of oxygen fugacity. *Geochim. Cosmochim. Acta* **74**, 5926–5938.

Kelley K. A. and Cottrell E. (2009) Water and the oxidation state of subduction zone magmas. *Science* **325**, 605–607.

Kinzler R. J. and Grove T. L. (1992) Primary magmas of mid-ocean ridge basalts 1. Experiments and methods.. *J. Geophys. Res.-Sol. Ea.* **97**, 6885–6906.

Klemme S., Gunther D., Hametner K., Prowatke S. and Zack T. (2006) The partitioning of trace elements between ilmenite, ulvospinel, armalcolite and silicate melts with implications for the early differentiation of the moon. *Chem. Geol.* **234**, 251–263.

Kloeck W. and Palme H. (1987) Partitioning of siderophile and chalcophile elements between metal, sulfide, olivine, and glass in a naturally reduced basalt from Disko Island, Greenland. *Lunar and Planetary Science Conference Proceedings* **18**, 471–483.

Kogiso T., Hirschmann M. M. and Frost D. J. (2003) High-pressure partial melting of garnet pyroxenite: possible mafic lithologies in the source of ocean island basalts. *Earth Planet. Sci. Lett.* **216**, 603–617.

Kogiso T., Hirschmann M. M. and Pertermann M. (2004) High-pressure partial melting of mafic lithologies in the mantle. *J. Petrol.* **45**, 2407–2422.

Kushiro I. (2001) Partial melting experiments on peridotite and origin of mid-ocean ridge basalt. *Annu. Rev. Earth Planet. Sci.* **29**, 71–107.

Langmuir C. H., Klein E. M. and Plank T. (1992) Petrological systematics of mid-ocean ridge basalts: constraints on melt generation beneath ocean ridges. *Geoph. Monogr. Ser.* **71**, 183–280.

Le Roux V., Lee C. T. A. and Turner S. J. (2010) Zn/Fe systematics in mafic and ultramafic systems: Implications for detecting major element heterogeneities in the Earth's mantle. *Geochim.*

Cosmochim. Acta **74**, 2779–2796.

Le Roux V., Dasgupta R. and Lee C. T. A. (2011) Mineralogical heterogeneities in the Earth's mantle: constraints from Mn Co, Ni and Zn partitioning during partial melting. *Earth Planet. Sci. Lett.* **307**, 395–408.

Lee C. T. A. (2002) Platinum-group element geochemistry of peridotite xenoliths from the Sierra Nevada and the Basin and Range. *California. Geochim. Cosmochim. Acta* **66**, 3987–4005.

Lee C.-T. A., Leeman W. P., Canil D. and Li Z.-X. A. (2005) Similar V/Sc systematics in MORB and arc basalts: implications for the oxygen fugacities of their mantle source regions. *J. Petrol.* **46**, 2313–2336.

Lee C.-T. A., Luffi P., Le Roux V., Dasgupta R., Albaréde F. and Leeman W. P. (2010) The redox state of arc mantle using Zn/Fe systematics. *Nature* **468**, 681–685.

Lee C. T. A., Luffi P., Chin E. J., Bouchet R., Dasgupta R., Morton D. M., Le Roux V., Yin Q. and Jin D. (2012) Copper systematics in arc magmas and implications for crust–mantle differentiation. *Science* **336**, 64–68.

Li Y. and Audétat A. (2012) Partitioning of V, Mn Co., Ni, Cu, Zn, As, Mo, Ag, Sn, Sb, W, Au, Pb, and Bi between sulfide phases and hydrous basanite melt at upper mantle conditions. *Earth Planet. Sci. Lett.* **355–356**, 327–340.

Lorand J. P. (1990) Are spinel lherzolite xenoliths representative of the abundance of sulfur in the upper mantle. *Geochim. Cosmochim. Acta* **54**, 1487–1492.

Mallik A. and Dasgupta R. (2012) Reaction between MORB-eclogite derived melts and fertile peridotite and generation of ocean island basalts. *Earth Planet. Sci. Lett.* **329**, 97–108.

Mattioli G. S. and Wood B. J. (1986) Upper mantle oxygen fugacity recorded by spinel lherzolites. *Nature* **322**, 626–628.

Mavrogenes J. A. and O'Neill H. S. C. (1999) The relative effects of pressure, temperature and oxygen fugacity on the solubility of sulfide in mafic magmas. *Geochim. Cosmochim. Acta* **63**, 1173–1180.

McInnes B. I. A., Gregoire M., Binns R. A., Herzig P. M. and Hannington M. D. (2001) Hydrous metasomatism of oceanic sub-arc mantle, Lihir, Papua New Guinea: petrology and geochemistry of fluid-metasomatised mantle wedge xenoliths. *Earth Planet. Sci. Lett.* **188**, 169–183.

Mckenzie D. and O'Nions R. K. (1995) The source regions of ocean island basalts. *J. Petrol.* **36**, 133–159.

Mungall J. E. (2002) Roasting the mantle: Slab melting and the genesis of major Au and Au-rich Cu deposits. *Geology* **30**, 915.

Mungall J. E., Hanley J. J., Arndt N. T. and Debecdelievre A. (2006) Evidence from meimechites and other low-degree mantle melts for redox controls on mantle-crust fractionation of platinum-group elements. *Proc. Natl. Acad. Sci. U.S.A.* **103**, 12695–12700.

Naldrett A. (1989) Experimental studies on sulfide, sulfide oxide, and sulfide silicate systems. *Oxford Monographs on Geology and Geophysics* **14**, 17–37.

Niu Y. (1997) Mantle melting and melt extraction processes beneath ocean ridges: evidence from abyssal peridotites. *J. Petrol.* **38**, 1047–1074.

Niu Y. L. and O'Hara M. J. (2008) Global correlations of ocean ridge basalt chemistry with axial depth: a new perspective. *J. Petrol.* **49**, 633–664.

Noll P. D., Newsom H. E., Leeman W. P. and Ryan J. G. (1996) The role of hydrothermal fluids in the production of subduction zone magmas: evidence from siderophile and chalcophile trace elements and boron. *Geochim. Cosmochim. Acta* **60**, 587–611.

O'Neill H. S. (1987) Quartz-fayalite-iron and quartz-fayalite-magnetite equilibria and the free energy of formation of fayalite (Fe_2SiO_4) and magnetite (Fe_3O_4). *Am. Mineral.* **72**, 67–75.

O'Neill H. S. C. (1991) The origin of the Moon and the early history of the Earth—a chemical model. Part 2: the Earth. *Geochim. Cosmochim. Acta* **55**, 1159–1172.

O'Neill H. S. C. and Pownceby M. I. (1993a) Thermodynamic data from redox reactions at high temperatures. I. An experimental and theoretical assessment of the electrochemical method using stabilized zirconia electrolytes, with revised values for the Fe-FeO, Co-CoO, Ni-NiO and Cu-Cu_2O oxygen buffers, and new data for the W-WO_2 buffer. *Contrib. Mineral. Petrol.* **114**, 296–314.

O'Neill H. S. C. and Pownceby M. I. (1993b) Thermodynamic data from redox reactions at high temperatures. II. The MnO-Mn_3O_4 oxygen buffer, and implications for the thermodynamic properties of MnO and Mn_3O_4 *Contrib. Mineral. Petrol.* **114**, 315–320.

Parkinson I. J. and Arculus R. J. (1999) The redox state of subduction zones: insights from arc-peridotites. *Chem. Geol.* **160**, 409–423.

Paster T. P., Schauwecker D. S. and Haskin L. A. (1974) The behavior of some trace elements during solidification of the Skaergaard layered series. *Geochim. Cosmochim. Acta* **38**, 1549–1577.

Pearce J. A. and Parkinson I. J. (1993) Trace element models for mantle melting: application to volcanic arc petrogenesis. *Geological Society, London, Special Publications* **76**, 373–403.

Pedersen A. K. (1979) Basaltic glass with high-temperature equilibrated immiscible sulphide bodies with native iron from Disko, central West Greenland. *Contrib. Mineral. Petrol.* **69**, 397–407.

Pilet S., Hernandez J., Bussy F. and Sylvester P. J. (2004) Short-term metasomatic control of Nb/Th ratios in the mantle sources of intraplate basalts. *Geology* **32**, 113–116.

Pilet S., Hernandez J., Sylvester P. and Poujol M. (2005) The metasomatic alternative for ocean island basalt chemical heterogeneity. *Earth Planet. Sci. Lett.* **236**, 148–166.

Pilet S., Baker M. B. and Stolper E. M. (2008) Metasomatized lithosphere and the origin of alkaline lavas. *Science* **320**, 916–919.

Plank T. and Langmuir C. H. (1988) An evaluation of the global variations in the major element chemistry of arc basalts. *Earth Planet. Sci. Lett.* **90**, 349–370.

Prouteau G. and Scaillet B. (2013) Experimental constraints on sulphur behaviour in subduction zones: Implications for TTG and adakite production and the global sulphur cycle since the Archean. *J. Petrol.* **54**, 183–213.

Putirka K., Ryerson F. J., Perfit M. and Ridley W. I. (2011) Mineralogy and composition of the oceanic mantle. *J. Petrol.* **52**, 279–313.

Ren Z.-Y., Takahashi E., Orihashi Y. and Johnson K. T. (2004) Petrogenesis of tholeiitic lavas from the submarine Hana Ridge, Haleakala volcano. *Hawaii. J. Petrol.* **45**, 2067–2099.

Ripley E. M. and Brophy J. G. (1995) Solubility of copper in a sulfur-free mafic melt. *Geochim. Cosmochim. Acta* **59**, 5027–5030.

Ripley E. M., Brophy J. G. and Li C. (2002) Copper solubility in a basaltic melt and sulfide liquid/silicate melt partition coefficients of Cu and Fe. *Geochim. Cosmochim. Acta* **66**, 2791–2800.

Rollinson H. R. (1993) *Using Geochemical Data: Evaluation, Presentation, Interpretation*. Longman Scientific & Technical Essex.

Rowe M. C., Kent A. J. R. and Nielsen R. L. (2009) Subduction influence on oxygen fugacity and trace and volatile elements in basalts across the cascade volcanic arc. *J. Petrol.* **50**, 61–91.

Sinclair W. (2007) *Porphyry deposits. Mineral Deposits of Canada: A Synthesis of Major Deposit-Types, District Metallogeny, the Evolution of Geological Provinces, and Exploration Methods:*

Geological Association of Canada, Mineral Deposits Division, Special Publication, **vol. 5**, pp. 223–243.

Sobolev A. V., Hofmann A. W., Sobolev S. V. and Nikogosian I. K. (2005) An olivine-free mantle source of Hawaiian shield basalts. *Nature* **434**, 590–597.

Sobolev A. V., Hofmann A. W., Kuzmin D. V., Yaxley G. M., Arndt N. T., Chung S. L., Danyushevsky L. V., Elliott T., Frey F. A., Garcia M. O., Gurenko A. A., Kamenetsky V. S., Kerr A. C., Krivolutskaya N. A., Matvienkov V. V., Nikogosian I. K., Rocholl A., Sigurdsson I. A., Sushchevskaya N. M. and Teklay M. (2007) The amount of recycled crust in sources of mantle-derived melts. *Science* **316**, 412–417.

Sun S. S. (1982) Chemical composition and origin of the Earth's primitive mantle. *Geochim. Cosmochim. Acta* **46**, 179–192.

Sun W. D., Arculus R. J., Bennett V. C., Eggins S. M. and Binns R. A. (2003) Evidence for rhenium enrichment in the mantle wedge from submarine arc-like volcanic glasses (Papua New Guinea). *Geology* **31**, 845–848.

Sun W., Arculus R. J., Kamenetsky V. S. and Binns R. A. (2004a) Release of gold-bearing fluids in convergent margin magmas prompted by magnetite crystallization. *Nature* **431**, 975–978.

Sun W. D., Bennett V. C. and Kamenetsky V. S. (2004b) The mechanism of Re enrichment in arc magmas: evidence from Lau Basin basaltic glasses and primitive melt inclusions. *Earth Planet. Sci. Lett.* **222**, 101–114.

Tatsumi Y., Sakuyama M., Fukuyama H. and Kushiro I. (1983) Generation of arc basalt magmas and thermal structure of the mantle wedge in subduction zones. *J. Geophys. Res.* **88**, 5815–5825.

Wallace P. J. (2001) Volcanic SO2 emissions and the abundance and distribution of exsolved gas in magma bodies. *J. Volcanol. Geoth. Res.* **108**, 85–106.

Wallace P. J. and Edmonds M. (2011) The sulfur budget in magmas: Evidence from melt inclusions, submarine glasses, and volcanic gas emissions. *Rev. Mineral. Geochem.* **73**, 215–246.

Walter M. J. (1998) Melting of garnet peridotite and the origin of komatiite and depleted lithosphere. *J. Petrol.* **39**, 29–60.

Wood B. J. (1991) Oxygen barometry of spinel peridotites. *Rev. Mineral.* **25**, 417–431.

Wood B. J. and Virgo D. (1989) Upper mantle oxidation state: Ferric iron contents of Iherzolite spinels by 57 Fe Mössbauer spectroscopy and resultant oxygen fugacities. *Geochim. Cosmochim. Acta* **53**, 1277–1291.

Workman R. K. and Hart S. R. (2005) Major and trace element composition of the depleted MORB mantle (DMM). *Earth Planet. Sci. Lett.* **231**, 53–72.

Yurimoto H. and Ohtani E. (1992) Element partitioning between majorite and liquid: a secondary ion mass spectrometric study. *Geophys. Res. Lett.* **19**, 17–20.

Zack T. and Brumm R. (1998) Ilmenite/liquid partition coefficients of 26 trace elements determined through ilmenite/clinopyroxene partitioning in garnet pyroxene. *Proceedings of the 7th International Kimberlite Conference. Cape Town: Red Roof Design.*

Zajacz Z. and Halter W. (2007) LA-ICPMS analyses of silicate melt inclusions in co-precipitated minerals: quantification, data analysis and mineral/melt partitioning. *Geochim. Cosmochim. Acta* **71**, 1021–1040.

Zajacz Z., Seo J. H., Candela P. A., Piccoli P. M. and Tossell J. A. (2011) The solubility of copper in high-temperature magmatic vapors: a quest for the significance of various chloride and sulfide complexes. *Geochim. Cosmochim. Acta* **75**, 2811–2827.

Zajacz Z., Candela P. A., Piccoli P. M., Walle M. and Sanchez-Valle C. (2012) Gold and copper in volatile saturated mafic to intermediate magmas: solubilities, partitioning, and implications for ore deposit formation. *Geochim. Cosmochim. Acta* **91**, 140–159.

Zajacz Z., Candela P. A., Piccoli P. M., Sanchez-Valle C. and Wälle M. (2013) Solubility and partitioning behavior of Au, Cu, Ag and reduced S in magmas. *Geochim. Cosmochim. Acta* **112**, 288–304.

Associate editor: Rajdeep Dasgupta